MONTHLY NOTICES of the Royal Astronomical Society

Spiral galaxies of the Virgo cluster: Eleven more intermediate-mass black hole candidates with an associated X-ray point-source

Journal:	*Monthly Notices of the Royal Astronomical Society*
Manuscript ID	MN-20-5071-MJ
Manuscript type:	Main Journal
Date Submitted by the Author:	16-Dec-2020
Complete List of Authors:	Graham, Alister; Swinburne University of Technology, Centre for Astrophysics & Supercomputing Soria, Roberto; University of the Chinese Academy of Sciences, College of Astronomy and Space Sciences; Curtin University, International Centre for Radio Astronomy Research; The University of Sydney, Sydney Institute for Astronomy, School of Physics Davis, Benjamin; Swinburne University of Technology, Centre for Astrophysics and Supercomputing; New York University - Abu Dhabi Campus, Center for Astro, Particle, and Planetary Physics Kolehmainen, Mari; Universite de Strasbourg, Observatoire Astronomique Maccarone, Tom; Texas Tech University, Department of Physics Miller-Jones, James; Curtin University of Technology, Curtin Institute of Radio Astronomy Motch, Christian; University of Strasbourg, Observatoire Astronomique Swartz, Doug; Universities Space Research Association, NASA Marshall Space Flight Center
Keywords:	galaxies: spiral < Galaxies, galaxies: active < Galaxies, galaxies: nuclei < Galaxies, galaxies: star clusters: general < Galaxies, (galaxies:) quasars: supermassive black holes < Galaxies, X-rays: galaxies < Resolved and unresolved sources as a function of wavelength

MNRAS 000, 1–22 (0000) Preprint 16 December 2020 Compiled using MNRAS LATEX style file v3.0

Spiral galaxies of the Virgo cluster: Eleven more intermediate-mass black hole candidates with an associated X-ray point-source

Alister W. Graham[1⋆], Roberto Soria[2,3,4], Benjamin L. Davis[1,5], Mari Kolehmainen[6], Thomas Maccarone[7], James Miller-Jones[3], Christian Motch[6], and Douglas A. Swartz[8]

[1] *Centre for Astrophysics and Supercomputing, Swinburne University of Technology, Hawthorn, VIC 3122, Australia*
[2] *College of Astronomy and Space Sciences, University of the Chinese Academy of Sciences, Beijing 100049, China*
[3] *International Centre for Radio Astronomy Research, Curtin University, GPO Box U1 987, Perth, WA 6845, Australia*
[4] *Sydney Institute for Astronomy, School of Physics A28, The University of Sydney, Sydney, NSW 2006, Australia*
[5] *Center for Astro, Particle, and Planetary Physics (CAP^3), New York University Abu Dhabi*
[6] *Observatoire Astronomique, Université de Strasbourg, CNRS, UMR 7550, 11 Rue de l'Université, F-67000 Strasbourg, France*
[7] *Department of Physics and Astronomy, Texas Tech University, Box 41051, Lubbock, TX 79409-1051, USA*
[8] *Astrophysics Office, NASA Marshall Space Flight Center, ZP12, Huntsville, AL 35812, USA*

Accepted XXX. Received YYY; in original form ZZZ

ABSTRACT

Building upon the five galaxies in the Virgo cluster with both a predicted black hole mass of less than $\approx 10^5$ M$_\odot$ and a centrally-located X-ray point-source, we report on new Chandra X-ray Observatory data from the Large Project "Spiral galaxies of the Virgo cluster". We reveal 11 more such galaxies and thereby triple the number of active intermediate-mass black hole (IMBH) candidates in the Virgo cluster. This amounts to a ∼40 per cent X-ray detection rate among the late-type spiral galaxies, compared to just 10 per cent for the dwarf early-type galaxies. In all five of the new galaxies for which the X-ray flux was strong enough to establish the X-ray spectral energy distribution, it is consistent with a power-law, and it is suggestive of a non-stellar-mass black hole in the source with the highest flux (NGC 4197: $L_X \approx 10^{40}$ erg s^{-1}) if the X-ray spectrum corresponds to the 'low/hard state'. Several sources reside within a nuclear star cluster, with such systems expected to be a rich source of gravitational radiation and tidal disruption events. NGC 4470 and NGC 4212 are exciting because their centres contain dual X-ray point-sources separated by 170 and 240 pc, respectively. NGC 4492 and NGC 4313 also contain dual X-ray sources with ∼0.5 kpc separation. Follow-up work to further probe the black hole masses, and prospects for spatially-resolving the spheres of gravitational influence around IMBHs, are discussed.

Key words: galaxies: spiral – galaxies: active – galaxies: nuclei – galaxies: star clusters: general – (galaxies:) quasars: supermassive black holes – X-rays: galaxies

1 INTRODUCTION

While galaxies suspected of harbouring a supermassive black hole (SMBH) with a mass of around 10^5–10^6 M$_\odot$ at their centre have long been identified (e.g. Filippenko & Sargent 1985; Ho et al. 1995; Greene & Ho 2007; Yuan et al. 2014; Graham & Scott 2015; Subramanian et al. 2016; Liu et al. 2018) — including POX 52 (Barth et al. 2004; Thornton et al. 2008), NGC 4395 (La Franca et al. 2015; den Brok et al. 2015; Brum et al. 2019) and NGC 404 (Davis et al. 2020) — there is an observational-dearth of centrally-located black holes with masses that are intermediate between stellar-mass black holes ($\lesssim 10^2$ M$_\odot$) and SMBHs ($\gtrsim 10^5$ M$_\odot$). However, this is gradually changing, with exciting finds in IRAS 01072+4954 (Valencia-S. et al. 2012), LEDA 87300 (Baldassare et al. 2015; Graham et al. 2016), NGC 205 (Nguyen et al. 2018, 2019), NGC 3319 (Jiang et al. 2018; Davis & Graham 2020), and the host galaxies of GW170817A (Za-

⋆ E-mail: AGraham@swin.edu.au

ckay et al. 2019), GW190521 (The LIGO Scientific Collaboration et al. 2020), and 3XMM J215022.4-055108 (Lin et al. 2020).

Indeed, the flood gates may be starting to open on the elusive 10^2-10^5 $M_\odot$ mass domain. Recently, Chilingarian et al. (2018) used the width and luminosity of the H_α emission line to identify intermediate-mass black hole (IMBH) candidates at the centres of 305 galaxies: ten of which have X-ray data that reveal a coincident point-source and suspected active galactic nucleus (AGN), and four of these ten (which includes LEDA 87300) have a black hole mass estimate less than $\sim 10^5$ $M_\odot$. In addition, Moran et al. (2014) has reported on 28 nearby (<80 Mpc) dwarf galaxies with narrow emission line (Type 2) AGN, while Mezcua et al. (2018, see their Figure 1) report on X-ray emission coming from 40 predominantly star-forming dwarf galaxies with Type 2 AGN out to a redshift of $\sim$1.3, with three galaxies stretching the sample out to $z = 2.39$. Mezcua et al. (2018, see their Figure 8) applied a roughly linear $M_{\rm bh}$–$M_{*,\rm gal}$ relation to the galaxy masses to predict that 7 of their 40 galaxies have black hole masses less than 10^5 $M_\odot$.

Closer to home, Graham & Soria (2019) and Graham et al. (2019, hereafter GSD19) have identified 63 Virgo cluster galaxies expected to house a central IMBH according to one or more black hole mass scaling relations, including the newer, morphology-dependent $M_{\rm bh}$–$M_{*,\rm gal}$ relations (Sahu et al. 2019a, , and references therein). Reanalysing the archival X-ray data for the 30 early-type galaxies in this set, Graham & Soria (2019) showed that three of them (IC: 3442, 3492 and 3292)[1] display a central X-ray point-source, while GSD19 reported that among the remaining 33 late-type galaxies, three (NGC: 4470, 4713 and 4178)[2] of the seven with archival X-ray data possessed a central X-ray point-source. Although, GSD19 noted that NGC 4178's X-ray source may be due to a stellar-mass black hole, and therfore, we do not count it here as a potential IMBH candidate. The higher activity ratio in the late-type spiral galaxies — when compared to the dwarf early-type galaxies (3/30) — may be related to higher gas fractions keeping on the AGN pilot light. Inactive IMBHs in dwarf early-type galaxies may, however, still be common (Silk 2017; Penny et al. 2018; Birchall et al. 2020). Of note is that both the early- and late-type samples contain dense nuclear star clusters (Ferrarese et al. 2006; Côté et al. 2006), therefore disfavouring X-ray binaries in nuclear star clusters as the the origin of the central X-ray point-sources, and favouring AGN.

It is common for the centres of galaxies to house a nuclear star cluster (Reaves 1983; Binggeli et al. 1985; Sandage et al. 1985; Carollo et al. 1997; Matthews et al. 1999; Böker et al. 2002). These clusters can reside in a more gas rich environment than globular clusters because their gas escape speed, due to the surrounding galaxy, is much higher than in globular clusters. Some nuclear star clusters also have radial light profiles with a high Sérsic index (Graham & Spitler 2009), and thus a steep inner density profile and gravitational gradient. Not surprisingly, galaxy centres are suspected to be ripe fields for cataclysmic disruptions and mergers of stars, neutron stars and black holes (e.g. Dokuchaev & Ozernoi 1981; Illarionov & Romanova 1988; Quinlan & Shapiro 1990; Pfister et al. 2020), and they may be the sites for some of the hard-to-spatially-constrain gravitational waves arising from the collision of compact massive objects (Abbott et al. 2016a,b; Andreoni et al. 2017; Abbott et al. 2018; Coughlin et al. 2019; The LIGO Scientific Collaboration et al. 2020), and also the ejection of high-velocity stars (e.g. Baumgardt et al. 2004; Levin 2006; Sesana et al. 2006; Koposov et al. 2020). As with massive black holes, the masses of nuclear star clusters were also discovered to correlate with the host spheroid mass (Balcells et al. 2003; Graham & Guzmán 2003). Furthermore, the coexistence of black holes and nuclear star clusters (Graham & Driver 2007; González Delgado et al. 2008; Seth et al. 2008; Graham & Spitler 2009; Graham 2016) implies the existence of a relation between black hole mass and nuclear star cluster mass, which is given by

$$\log\left(\frac{M_{\rm bh}}{\rm M_\odot}\right) = (2.62\pm0.42)\log\left(\frac{M_{\rm nc}}{10^{7.83}\,\rm M_\odot}\right) + (8.22\pm0.20) \quad (1)$$

(Graham 2016, 2020). This relation holds in the absence of a galaxy bulge, making it a useful tool for late-type spiral galaxies, as are the more familiar $M_{\rm bh}$–$M_{*,\rm gal}$, $M_{\rm bh}$–σ, and $M_{\rm bh}$–ϕ relations (Hutchings et al. 1984; Yee 1992; Merritt 2000; Ferrarese & Merritt 2000; Gebhardt et al. 2000; Seigar et al. 2008; Davis et al. 2017, 2018; Sahu et al. 2019b).

Through a *Chandra X-ray Observatory* (*CXO*) Large Project, we have obtained X-ray data for the 26 previously unobserved Virgo cluster spiral galaxies predicted to house an IMBH. In Section 2, we introduce the subsample which was found to have a centrally-located X-ray point-source, and thus probable AGN. Results for the spiral galaxies with expected black hole masses greater than 10^5–10^6 $M_\odot$ will be presented in a subsequent paper exploring AGN occupation fractions, Eddington ratios, and trends with the host galaxy mass. In Section 3, we report on the X-ray data for this subsample of active IMBH candidates, while Section 4 discusses the prospects for estimating the black hole mass using the X-ray data alone (subsection 4.1) or when combined with radio data (subsection 4.2). Section 5 reviews expectations for spatially resolving the gravitational sphere-of-influence around IMBHs, and provides some direction for future observations of the IMBH candidates identified here.

[1] X-ray point-source discovery in IC 3442 and IC 3492 was by Gallo et al. (2010).
[2] X-ray point-source discovery in NGC 4713 was by Terashima et al. (2015), and in NGC 4178 by Secrest et al. (2012).

Table 1. IMBH mass predictions based on the host galaxy properties

Galaxy	D [Mpc]	$\log M_{\rm bh}$ ($M_{*,\rm total}$)	$\log M_{\rm bh}$ (ϕ)	$\log M_{\rm bh}$ (σ)	$\log M_{\rm bh}$ ($M_{\rm nc}$)	$\overline{\log M_{\rm bh}}$
Archival X-ray data presented in Graham et al. (2019)						
N4178	13.20±3.00	3.9±0.9	4.2±1.6	3.1±0.9	2.6±1.6	3.5±0.6
N4713	14.80±3.55	3.8±0.9	3.5±1.9	2.8±1.3	4.6±1.7	3.6±0.6
N4470	16.40±6.60	3.4±1.2	4.6±2.6	5.1±0.8[a]	4.5±1.7	4.6±0.6
New X-ray data						
N4197	26.40±3.92	4.3±0.8	5.4±0.9	...	...	4.8±0.6
N4212	17.05±2.62	6.0±0.9	5.9±0.4	5.1±0.8	6.2±1.6	5.8±0.3
N4298	15.80±2.54	5.3±0.8	5.6±0.8	4.2±0.8	5.3±1.7	5.1±0.4
N4313	14.15±2.92	4.9±0.9	...	5.2±0.8	6.7±1.6	5.3±0.6
N4330	19.30±1.56	4.4±0.8	...	...	...	4.4±0.8
N4492[b]	19.30±3.54	4.9±0.9	...	...	...	4.9±0.9
N4498	14.55±3.62	3.7±0.9	5.8±1.8	...	3.8±1.5	4.0±0.7
N4519	19.60±8.48	4.2±1.2	5.5±2.3	...	...	4.5±1.1
N4607	19.70±6.55	4.5±1.1	...	...	...	4.5±1.1
N4405	17.85±3.32	4.4±0.9	...	...	...	4.4±0.9
N4413	16.05±1.40	3.7±0.8	4.5±0.6	...	...	4.2±0.5

Black hole masses are in units of solar mass, derived from one to four independent observables (see Section 2.2) depending on their availability: $M_{*,\rm total}$, ϕ, σ, and $M_{\rm nc}$. [a] Revised down from $10^6\,{\rm M}_\odot$ in GSD19 due to the velocity dispersion dropping from 90 to ∼60 km s^{-1} (see Section 3.3.3). [b] NGC 4492 has archival *CXO* data, but is new in the sense that we did not report on the X-ray data in GSD19.

2 THE SAMPLE AND THEIR EXPECTED BLACK HOLE MASSES

2.1 The sample

The abundance of SMBHs at the centres of galaxies has led to many black hole mass scaling relations, some of which, including the above mentioned $M_{\rm bh}$–$M_{\rm nc}$ relation, were recently used by us to estimate the masses of the black holes at the centres of 100 early-type galaxies (Graham & Soria 2019) and 74 late-type galaxies (GSD19) in the Virgo galaxy cluster. The early-type galaxy sample was compiled by Côté et al. (2004) and the subsequent *CXO* images from the Large Project titled 'The Duty Cycle of Supermassive Black Holes: X-raying Virgo' (PI: T.Treu, Proposal ID: 08900784) were used to identify which galaxies had AGN (Gallo et al. 2010). We have established a complementary *CXO* Large Project titled 'Spiral galaxies of the Virgo Cluster' (PI: R.Soria, Proposal ID: 18620568) which has imaged 52 galaxies and utilised an additional 22 (+1=23)[3] spiral galaxies for which suitable archival X-ray data existed. The combined sample of spiral galaxies encapsulates all 75 Virgo cluster spiral galaxies with star-formation rates higher than $\sim 0.3\,{\rm M}_\odot\ {\rm yr}^{-1}$. We are following-up on GSD19, who determined that 33 of the original 74 spiral galaxies are expected to harbour a central IMBH based upon the $M_{\rm bh}$–ϕ and $M_{\rm bh}$–σ relation (Davis et al. 2017), and the $M_{\rm bh}$–$M_{*,\rm galaxy}$ relation for spiral galaxies (Davis et al. 2018).

This paper pertains to the (33-7=) 26 spiral galaxies predicted to have an IMBH but which did not previously have archival X-ray data.[4] More specifically, of these 26 spiral galaxies, we will focus on those found here to have a centrally-located X-ray point-source. We have discovered such sources in eight of these galaxies, giving a tally of nine new detections when including NGC 4492 (see footnote 3). Furthermore, we report on NGC 4405 and NGC 4413, both containing nuclear X-ray emission which is likley from a point-source — although the low source count makes this less certain — thereby taking the total to 11 galaxies. For convenience of reference, all of these galaxies, and their predicted black hole masses, are presented in Table 1. This table also includes the three pre-existing galaxies from GSD19 which we report a little further on in the next section.

It is worth noting that, combined with the previous two Virgo cluster spiral galaxies which have a centrally-located X-ray point-source and a predicted black hole mass less than $10^5\,{\rm M}_\odot$ (GSD19), we now have 13 such detections from the initial pool of 33 Virgo cluster spiral galaxies predicted to harbour an IMBH. This is roughly 4 times higher than the value of 10 per cent found by Graham & Soria (2019) among the 30 Virgo cluster dwarf early-type galaxies expected to have an IMBH and similarly imaged through a *CXO* Large Project with long exposure times. The more gas rich environment of the star-forming, late-type spiral galaxies is likely to be more favourable for igniting the central black hole and turning on the AGN than within the dwarf early-type galaxies. It also implies that we are probably not detecting X-ray binary systems (XRBs) involving compact stellar-mass objects (e.g. Casares et al. 1992; Soria & Wu 2003; Casares et al. 2014) because it would require a relatively high occupancy of an XRB at the centre of the late-type galaxies but not in the early-type galaxies (see also She et al. 2017). That is to say, the occurrence of (XRBs in) nuclear star clusters, which are prevalent in both types of galaxy, does not appear to be the driver of the X-ray point-source emission.

In passing, it is relevant to again note that using powerful data mining techniques, Chilingarian et al. (2018) searched the Chandra X-ray Observatory archives and identified a sample of 305 galaxies with both a Type I AGN, as determined from their optical spectra, and a suspected IMBH in the range $3 \times 10^4 < M_{\rm bh}/{\rm M}_\odot < 2 \times 10^5$. Ten

[3] We have discovered a central X-ray point-source in archival, Cycle 8, *CXO* data for NGC 4492, an additional Virgo spiral galaxy which is expected to harbour an IMBH, and which has taken our parent sample to 75 spiral galaxies.
[4] The seven spiral galaxies which did have archival data were reported on in GSD19.

of these galaxies were reported to have nuclear X-ray emission, and 4 of these 10 had one black hole mass estimate less than 10^5 M$_\odot$. Of these four galaxies, and of relevance here, is that the one with the smallest black hole mass estimate is the Virgo Cluster Catalog dwarf galaxy VCC 1019 (SDSS J122732.18+075747.7) imaged by *XMM-Newton*. However, we downloaded and reprocessed the *CXO* data for VCC 1019 — which is actually a background spiral galaxy at 150 Mpc — and found no X-ray emission, whereas Chilingarian et al. (2018) reported a "very faint" source.

2.2 The black hole masses

There are now many approaches to predict a galaxy's central black hole mass which do not rely upon the assumption of stable (virialised) gas clouds orbiting the black hole in some universal geometrical configuration. This approach, used by Chilingarian et al. (2018), employs a sample mean virial factor, $\langle f \rangle$, obtained by linking (reverberation mapping)-derived virial products (e.g., Peterson & Wandel 2000) to either the $M_{\rm bh}$–σ or $M_{\rm bh}$–$M_{*,\rm gal}$ relation defined by galaxies with directly measured black hole masses $\gtrsim 10^6$ M$_\odot$ (Onken et al. 2004; Graham et al. 2011). In GSD19, we instead predicted the central black hole masses of our Virgo sample of spiral galaxies directly from the $M_{\rm bh}$–σ and $M_{\rm bh}$–$M_{*,\rm gal}$ relations, which have a total root mean square (and intrinsic) scatter of 0.63 (0.51±0.04) and 0.79 (0.69) dex, respectively, in the log $M_{\rm bh}$-direction. We additionally predicted the black hole mass using the host galaxy's spiral arm pitch angle, ϕ, via the $M_{\rm bh}$–ϕ relation which has the smallest scatter of all the black hole scaling relations at just 0.43 (0.30±0.08) dex (Davis et al. 2017). We then highlighted galaxies for which multiple methods, from independent observations (σ, $M_{*,\rm gal}$, ϕ), consistently yielded an expectation of an *intermediate-mass* black hole. Given the absence of bulges in some late-type spiral galaxies with massive black holes, and the somewhat comparable levels of scatter about the $M_{\rm bh}$–$M_{*,\rm gal}$ ($\Delta_{\rm rms,total} = 0.79$ dex Davis et al. 2018) and $M_{\rm bh}$–$M_{*,\rm bulge}$ ($\Delta_{\rm rms,total} = 0.64 - 0.66$ dex Davis et al. 2019) relations for spiral galaxies, we have not used the $M_{\rm bh}$–$M_{*,\rm bulge}$ relation.

For reference, the nucleated Sérsic galaxy NGC 205 has the lowest directly measured black hole mass, at $(7.1^{+10.7}_{-5.3}) \times 10^3$ M$_\odot$ (Nguyen et al. 2019, their Table 6). With a stellar velocity dispersion of 33 km s^{-1} from HyperLeda[5] (Paturel et al. 2003), NGC 205 agrees well with, and thus extends, the $M_{\rm bh}$–σ relation for Sérsic, and thus spiral, galaxies into the 10^3–10^4 M$_\odot$ range (Sahu et al. 2019b, see their Figures 3 and 11). The dwarf S0 galaxy NGC 404, with a reported black hole mass equal to $(7^{+1.5}_{-2.0}) \times 10^4$ M$_\odot$ (Nguyen et al. 2017), also follows the $M_{\rm bh}$–σ relation for Sérsic galaxies (Sahu et al. 2019b, their Figures 2 and 3). Having a well-resolved nuclear star cluster, with a mass of $(1.8 \pm 0.8) \times 10^6$ M$_\odot$ (Graham & Spitler 2009; Nguyen et al. 2018), NGC 205 also agrees well with and extends the $M_{\rm bh}$–$M_{\rm nc}$ relation into this lower mass range (Graham 2020).

We have revised some of the predicted black hole masses from GSD19 that were based on the $M_{\rm bh}$–$M_{*,\rm gal}$ relation due to our use of the median, rather than the mean, redshift-independent distance in the NASA/IPAC Extragalactic Database (NED)[6]. For each galaxy, we inspected the histogram of distances, and for some we removed outliers and re-derived the median value, which is listed in Table 1. The revised distances impact upon the absolute magnitudes and in turn the stellar-mass of each galaxy, and thus the predicted black hole masses. For the nucleated galaxies, i.e. those with nuclear star clusters, we also include the estimate of the central black hole mass derived from the nuclear star cluster mass (see equation 1).

A nuclear star cluster is known to reside in a couple of the spiral galaxies with both (i) a central X-ray point-source and (ii) a suspected IMBH. The reported nuclear star cluster mass for NGC 4178 (5×10^5 M$_\odot$: Satyapal et al. 2009) is assumed to have an accuracy of a factor of 2. Although Satyapal et al. (2009) report that NGC 4713 also contains a nuclear star cluster, or at least a point-like source (possibly contaminated by AGN light), they refrain from providing a mass measurement. In NGC 4498, the Johnson/Cousins V-band apparent magnitude of the nuclear star cluster has been reported as 21.53 ± 0.02 mag (Georgiev & Böker 2014), and the stellar-mass for the nuclear star cluster has been taken as $(1.4 \pm 0.4) \times 10^6$ M$_\odot$ from Georgiev et al. (2016, their Table A1). The expected black hole masses, based upon these nuclear star cluster masses, are calculated here using equation 1, taken from Graham (2020, their equation 7), which is more accurate than the previous estimates obtained from the inverse of equation 12 in GSD19. This $M_{\rm bh}$–$M_{\rm nc}$ relation is applicable[7] for $10^5 \lesssim M_{\rm nc}/M_\odot \lesssim 5 \times 10^7$, and has an uncertainty calculated using the expression

$$[\delta \log(M_{\rm bh}/{\rm M}_\odot)]^2 = \left[\log\left(\frac{M_{\rm nc}}{10^{7.83}\,{\rm M}_\odot}\right)\right]^2 (0.42)^2 \left(\frac{2.62}{\ln 10}\right)^2 \left(\frac{\delta M_{\rm nc}}{M_{\rm nc}}\right)^2 + (0.20)^2 + (\delta_{\rm int})^2, \quad (2)$$

where the intrinsic scatter within the $M_{\rm bh}$–$M_{\rm nc}$ relation, $\delta_{\rm int}$, has been taken to be 1.31 dex (Graham 2020). The results are given in Table 1.

A novel approach employed by Davis & Graham (2020) in the case of NGC 3319 was to determine the error-weighted mass from many independent black hole mass estimates, $\log(M_{{\rm bh},i})$. Accounting for each estimate's associated uncertainty, $\delta \log(M_{{\rm bh},i})$, the combined probability distribution function (PDF) yields the statistically most likely value (and its 1σ uncertainty range) for the black hole mass of each galaxy. When many such independent estimates are brought to bear on this derivation, as was the case for NGC 3319, one has a rather well-defined (Gaussian-like) PDF from which one can readily establish the probability of having detected an IMBH with $M_{\rm bh} < 10^5$ M$_\odot$. Here, with fewer estimates per galaxy, we proceed along a simpler path by determining the error-weighted mean of the logarithm of the black hole masses, such that

$$\overline{\log M_{\rm bh}} = \frac{\sum_{i=1}^{N} w_i \log M_{{\rm bh},i}}{\sum_{i=1}^{N} w_i}, \quad (3)$$

[5] http://leda.univ-lyon1.fr

[6] http://nedwww.ipac.caltech.edu

[7] The upper mass cut excludes systems with half-light radii greater than ∼20 pc, which may be regarded as nuclear discs rather than ellipsoidal-shaped star clusters.

where we have used inverse-variance weighting[8] and thus $w_i = 1/(\delta \log M_{\rm bh,}{}_i)^2$. The 1σ standard error bar attached to this mean is calculated as

$$\delta\,\overline{\log M_{\rm bh}} = \sqrt{\frac{1}{\sum_{i=1}^{N} w_i}}. \quad (4)$$

Table 1 provides the mean black hole mass estimates for our sample of late-type galaxies possessing a centrally-located X-ray point-source. With the exception of NGC 4212, with dual X-ray point-source, the estimates are typicaly less than $\sim 10^5$ M$_\odot$.

3 THE X-RAY DATA & ANALYSIS

3.1 Nuclear source detection

The *CXO's* Advanced CCD Imaging Spectrometer (ACIS) data were obtained under the 'Spiral galaxies of the Virgo Cluster' Large Project (Proposal ID: 18620568). In addition, we used archival observations for some of the target galaxies. We analysed the data in a consistent manner with GSD19, employing the Chandra Interactive Analysis of Observations (CIAO) Version 4.12 software package (Fruscione et al. 2006), and Calibration Database Version 4.9.1. We reprocessed the event files of every observation with the CIAO task *chandra_repro*. For galaxies with multiple observations, we created merged event files with *reproject_obs*. In those cases, we used the stacked images to improve the signal-to-noise ratio in our search for possible nuclear sources; however, the fluxes from the nuclear candidates were then estimated from the individual exposures.

We used the coordinate position of the galactic nuclei reported in NED as a reference position for our search of nuclear X-ray sources. We looked for significant X-ray emission within $2''$ of the reference nuclear location. The fact that we knew in advance the (approximate) position of the sources we were looking for means that we could identify significant detections with a far lower number of counts than we would require from a blind source-finding task (e.g., *wavdetect*). That, combined with the very low background level in the ACIS images, results in 99% significant detections even for sources with as few as 5 counts (e.g., see the Bayesian confidence intervals in Kraft et al. 1991). As a rough estimate, 5 ACIS-S counts in a typical 10 ks exposure, correspond to a 0.5–10 kev luminosity of $\sim 2 \times 10^{38}$ erg s^{-1} at a distance of 17 Mpc.

When significant emission was detected at the nuclear position, we estimated whether the source was consistent with being point-like, or was instead significantly more extended than the instrumental point-spread-function (PSF) of the ACIS detector at that location (in most cases, close to the aim-point of the S3 chip). In cases where we determined that the emission was extended, we inspected the images in the soft (0.3–1 keV), medium (1–2 keV) and hard (2–10 keV) bands separately. This enabled us to determine whether there was a point-like (harder) X-ray source surrounded by diffuse thermal emission, characteristic of star-forming regions; typically, the latter does not significantly contribute to the 2–10 keV band.

For all nuclear point-like sources, we defined source extraction regions with a radius suitable to the size of the PSF (typically, a circle with $2''$ radius for sources at the aim-point of the S3 chip) and local background regions at least 4 times larger than the source region. We visually inspected all source and background regions to make sure they did not contain other contaminating sources. In all cases, we ran the CIAO task *srcflux* to estimate the absorbed and unabsorbed fluxes. The PSF fraction in the extraction circle was estimated with the *srcflux* option 'psfmethod=arfcorr', which essentially performs a correction to infinite aperture. In some cases, when the count rate was high enough, we also extracted the source spectra and modelled them in XSPEC, as described next.

3.2 Flux and luminosity of detected nuclear sources

The task *srcflux* provides two alternative estimates of the absorbed X-ray flux: model fluxes and model-independent fluxes. Both values can be described as approximations to the ideal "observed" flux that would be measurable from a dataset with an infinitely high signal-to-noise. For the model fluxes, we assumed a power-law spectrum with photon index $\Gamma = 1.7$ and Galactic line-of-sight column density of H I gas (HI4PI Collaboration et al. 2016), taken from the High Energy Astrophysics Science Archive Research Center (HEASARC)[9]. More realistically, even for nuclear sources with the least amount of intrinsic absorption, we may expect a total $N_{\rm H}$ value which is a factor of 2 higher than the Galactic $N_{\rm H}$ value, owing to the absorbing matter in the host Virgo spiral galaxy; this conversion factor would depend on the size and Hubble type of the host galaxy, on its metallicity and star formation rate, and on our viewing angle. However, the difference in the estimated unabsorbed luminosities corrected for a column density of, for example, $\sim 4 \times 10^{20}$ cm^{-2} as opposed to $\sim 2 \times 10^{20}$ cm^{-2} is only about 4 percent (well below the other observational and systematic uncertainties), because such column densities block photons only at the low end of the ACIS-S energy range, where the instrumental sensitivity is already very low. Thus, we avoided those complications, because they are largely irrelevant for the purpose of this work, and list the unabsorbed luminosities as corrected only for Galactic $N_{\rm H}$ in all cases when there are not enough counts for any significant estimate of $N_{\rm H,int}$ (as explained later). It is simple to estimate the fluxes and luminosities of the same sources corrected for higher values of $N_{\rm H}$ (if so desired), with the Portable Interactive Multi-Mission Software (PIMMS)[10].

Model-independent fluxes from *srcflux* are based on the energy of the detected photons, convolved by the detector response. For sources with a small number of counts, the detected photons may not uniformly sample the energy range,

[8] This weighting gives the 'maximum likelihood estimate' for the mean of the probability distributions under the assumption that they are independent and normally distributed with the same mean.

[9] https://heasarc.gsfc.nasa.gov/cgi-bin/Tools/w3nh/w3nh.pl

[10] http://asc.harvard.edu/toolkit/pimms.jsp

especially at higher energies (lower sensitivity): thus, the model-independent flux is not necessarily a more accurate approximation of the "ideal" observable flux than the model-dependent value. Moreover, we need the model-dependent fluxes in order to estimate the unabsorbed fluxes and luminosities, a conversion that cannot be done directly from the model-independent fluxes. In most cases in our sample of nuclear sources, the model-dependent and independent fluxes agree within the error bars. However, when they differ significantly, it is a clue that either our assumed power-law is wrong, or that the column density is $>10^{20}$ cm^{-2}. We flagged those cases for further analysis with XSPEC.

In order to mitigate the effect of an uncertain $N_{\rm H}$ on our estimate of the unabsorbed flux and luminosity, we computed model-dependent fluxes with *srcflux* in the 1.5–7 kev band rather than in the "broad" 0.5–7 keV band. This is because photo-electric absorption is negligible above 1.5 keV, at least for the range of column densities seen in Virgo spirals (up to a few 10^{22} cm^{-2}). Thus, the observed count rate at 1.5–7 keV provides a more accurate normalization of the true power-law spectrum. We then compute the 0.5-7 keV flux by extrapolating the power-law model to lower energies.

There is a second reason why it is more convenient to use the 1.5-7 keV band rather than the full ACIS band for an estimate of the nuclear fluxes with *srcflux*. Some nuclei may have thermal plasma emission from diffuse hot gas (for example caused by star formation in the nuclear region) in addition to point-like emission from the central black hole. Spatial separation of the diffuse and point-like components is often impossible; two-component modelling is also not an option for low-count spectra from sources with luminosities $\lesssim 10^{40}$ erg s^{-1} at the distance of the Virgo Cluster. Instead, it is plausible to assume that the power-law component from the nuclear black hole dominates above 1.5 keV, and the ∼0.5-keV thermal plasma emission affects mostly the softer band. By normalizing the power-law model to the 1.5-7 keV flux and extrapolating it down to lower energies, we obtain a more accurate estimate of the nuclear emission than if we fit the power-law model over the whole 0.5–7 keV range.

In Table 3, one can find the model-independent fluxes of all the sources, and the model-dependent fluxes and luminosities of the sources, computed with *srcflux*. We converted unabsorbed 0.5-7 keV fluxes to unabsorbed luminosities in the same band assuming the distances reported in Table 1. Finally, we converted luminosities across different bands using PIMMS, with the assumed power-law model.

We carried out a full spectral analysis for those nuclear sources with a sufficient number of counts, and for sources in which our preliminary *srcflux* analysis and our inspection of the X-ray colours suggested evidence of a high absorbing column density. We extracted spectra and associated response and ancillary response files with the CIAO task *specextract*. We then regrouped the spectra to 1 count per bin with the task *grppha* from the FTOOLS software (Blackburn 1995), and modelled them in XSPEC version 12.9.1 (Arnaud 1996), using the Cash (1979) statistics. The count rate is generally too low for complex modelling; however, we can spot cases of high $N_{\rm H,int}$ and constrain its value even for sources with as low as a dozen counts, because those counts would all be recorded at energies >1 keV. The second parameter left free in our XSPEC fitting is the power-law normalization. In a few cases, we had enough counts to leave also the photon index as a free parameter; in most other cases, we fixed it at the canonical value of 1.7. In one case, NGC 4178, the best-fitting power-law model is very steep (Table 3), and the disk-blackbody model *diskbb* provides a more physical (although statistically equivalent) fit. Finally, for the sources modelled in XSPEC, we determined the 90% confidence limits on their absorbed and unabsorbed model fluxes (and hence, on their unabsorbed luminosities) with the convolution model *cflux*.

3.3 Galaxies with archived X-ray data reported in GSD19

Three galaxies (NGC 4178, NGC 4713, and NGC 4470) from GDS19 had both archival X-ray data revealing a central X-ray point-source and at least two estimates for $M_{\rm bh} < 10^5\,{\rm M}_\odot$. NGC 4178 (GSD19, their Figure 11) appears to represent a somewhat edge-on counterpart to NGC 4713 (GSD19, their Figure 13), for which some additional comments are provided next. In the case of NGC 4470, it was not the primary target of the past *CXO* observations, and as such it was always located several arcminutes from the aim-point, resulting in a broadened Point Spread Function (PSF) at this galaxy's centre. Below, we present the X-ray contours for NGC 4470, not previously shown in GSD19.

3.3.1 NGC 4178: blackbody versus power-law

As noted, NGC 4178 was presented in GSD19. Attempts to fit a power-law model to the X-ray SED, with its rapid drop off from the soft to the hard energy band, resulted in an unrealistically steep slope (see Table 3). The X-ray SED was instead quite well fit with a blackbody disk model having an intrinsic temperature $\rm T_{intrin}$ $0.56^{+0.35}_{-0.19}$ keV. The inner-disk radius $R_{\rm in}$ associated with the *diskbb* fit is such that $R_{\rm in}(\cos\theta)^{1/2} \approx 1.19 N_{\rm dbb}^{1/2}\, d_{10}$. With $N_{\rm dbb}$ the normalization of the *diskbb* model in XSPEC, d_{10} the distance to the source in units of 10 kpc, and θ our viewing angle ($\theta = 0$ is face-on), we obtain $R_{\rm in}(\cos\theta)^{1/2} \approx 104$ km (53–613 km, 90% confidence).

We compared the power-law and disk-blackbody models using the Anderson-Darling (AD) test statistics (e.g. Arnaud et al. 2011). Specifically, we performed Monte Carlo calculations of the goodness-of-fit in XSPEC, with the command *goodness*, and compared the percentage of simulations with the test statistic less than that for the data. For the power-law model, 75% of the realizations were better than the AD test value for the data (log AD = −3.67). For the disk-blackbody model, 43% of realizations were better than the AD value (log AD = −3.88). Thus, the disk-blackbody model is only weakly preferred.

3.3.2 NGC 4713: a LEDA 87300 analog

Both the image of NGC 4713 (GSD19, their Figure 13) and its light profile (Figure 1), resembles LEDA 87300 (Baldassare et al. 2015; Graham et al. 2016, see their Figures 2 and 5). From Hubble Space Telescope (*HST*) images, both galaxies can be seen to contain a central point-source and a bar with spiral arms emanating from the ends (Baldassare et al. 2017). The better spatial resolution provided by *HST* has removed the uncertain distinction between any bar plus

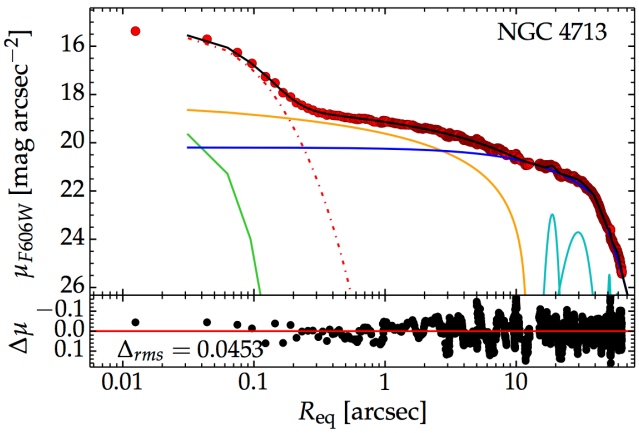

Figure 1. Geometric-mean axis, aka equivalent-axis light profile for the bulgeless galaxy NGC 4713, fit with a truncated exponential disk (dark blue) plus some faint spiral arm-crossings (light blue), a bar (orange), a nuclear star cluster (dot-dash red) and a very faint point-source (green).

bulge components — collectively referred to as the 'barge' (Graham et al. 2016) — that was previously affecting the ground-based images, with both galaxies now appearing to be bulgeless. The centrally-located point-source in the optical image of LEDA 87300 may be partly due to its active galactic nucleus (AGN), which was bright enough to enable Ho et al. (1997) to flag this galaxy as having a transition nucleus with a luminosity-weighted [OI] strength intermediate between HII nuclei and LINERS (low-ionisation nuclear emission-line regions). NGC 4713 was subsequently flagged by Decarli et al. (2007) as having a LINER/HII nucleus.

We have modelled the radial distribution of light in NGC 4713, and found that it contains a slightly resolved nuclear star cluster with an equivalent-axis half light radius equal to 0″.07 (5 pc), a Sérsic index $n = 1.23$, and an *F606W* apparent magnitude of 19.57±0.18 mag. Correcting for Galactic extinction, and using a stellar mass-to-light ratio[11] of 1.0±0.5, we obtain $\log(M_{nc}/M_\odot) = 6.43 \pm 0.31$ and a predicted black hole mass $\log(M_{bh}/M_\odot) = 4.56 \pm 1.66$. If the AGN point-source is brighter than that shown in Figure 1, then the nuclear star cluster will be fainter and the predicted black hole mass will be smaller. This may explain why this prediction is an order of magnitude higher than predicted by other methods (see Table 1.

LEDA 87300 is of interest because of its AGN, evidenced by its nuclear X-ray point-source, broad H_α emission, and narrow emission line ratios (Baldassare et al. 2015). Using a virial f-factor of $2.3^{+0.9}_{-0.6}$ from Graham et al. (2011) gives a virial black hole mass of $2.9^{+6.7}_{-2.3} \times 10^4 f_{2.3}$ $M_\odot$ (Graham et al. 2016). The heightened uncertainty on the black hole mass, with its 1σ error range from 0.6×10^4 to 10^5, is because the f-factor is the mean value derived from ∼30 AGN with reverberation mappings, and when using this value to predict the virial black hole mass for an individual galaxy like LEDA 87300, in addition to the observational measurement errors, one needs to fold in the intrinsic scatter between the individual AGN, which is roughly a factor of 3, coming from the scatter in the M_{bh}–σ diagram.

While LEDA 87300 has a stellar-mass of 2.4×10^9 $M_\odot$ (accurate to a factor of 2) and an estimated stellar velocity dispersion of 40 ± 11 km s^{-1} (Graham et al. 2016, see their section 3.2), NGC 4713 has a stellar-mass of 4×10^9 $M_\odot$ (GSD19) and a measured velocity dispersion of 23.2 ± 8.9 km s^{-1} (Ho et al. 2009). We will endeavour to obtain optical spectra of NGC 4713 to detect a broad H_α line. From this, we would be able to derive a virial mass for the black hole in NGC 4713 associated with the nuclear X-ray point-source and LINER/HII nucleus. As noted in GSD19, the X-ray photons from the central point-source in the archived *CXO*/ACIS-S image of NGC 4713 were detected in all three standard bands (soft, 0.3-1 keV; medium, 1-2 keV; hard, 2-7 keV), consistent with a power-law spectrum rather than purely a blackbody spectrum.

3.3.3 NGC 4470: dual X-ray point sources 170 pc apart

NGC 4470 is a face-on spiral galaxy (Figure 2). The Reference Catalog of galaxy Spectral Energy Distributions (RCSED: Chilingarian et al. 2017)[12] places NGC 4470 in the H_{II} region of the narrow-line $[O_{III}]/H_\beta$ versus $[N_{II}]/H_\alpha$ diagnostic diagram. However, it is becoming increasingly apparent that faint or 'hidden' AGN can be missed when using BPT (Baldwin et al. 1981) diagnostic diagrams (e.g. Zezas et al. 2005; Sartori et al. 2015; Lamperti et al. 2017; Cann et al. 2019). This is perhaps not surprising in low-mass galaxies because, unless the Eddington ratio is high, the AGN signal in the central aperture/fibre/spaxel will be increasingly swamped by the galaxy's star light in these systems with low black hole masses. Although, by concentrating on a nearby ($D \leq 80$ Mpc) sample of dwarf galaxies, Moran et al. (2014) did find 28 galaxies dominated by narrow emission line (Type 2) AGN, and assuming an [OIII]-to-bolometric luminosity correction factor of 1000 they reported minimum black hole masses of 10^3–10^6 $M_\odot$ for their sample.

The RCSED reports a velocity dispersion of 61 ± 6 km s^{-1} for NGC 4470 (SDSS J122937.77+074927.1). This is lower than the value of 90 ± 13.5 km s^{-1} that was used in GSD19, and results in a lower (M_{bh}–σ)-derived black hole mass of $\log M_{bh} = 5.1 \pm 0.8$. This mass is now consistent (overlapping uncertainties) with the (M_{bh}–$M_{*,gal}$)-derived value of $\log M_{bh} = 4.1 \pm 1.0$ (GSD19).

Given that the pre-existing *CXO* data for NGC 4470 was (intentionally)[13] offset from the aim-point of the telescope, it required a careful re-analysis. Six of the past seven ACIS observations (spanning 2010 to 2019) only captured the nuclear region of NGC 4470 on the external chips, where the PSF was unfortunately too broad and distorted to obtain a reliable flux measurement. However, a ∼20 ks exposure from 2010 (*CXO* Obs. ID 12978), directed 4 arcminutes away at the globular cluster RZ 2109 around NGC 4472, proved fruitful, and we have re-analysed these data to report on NGC 4470's central X-ray point-source (Table 3).

[11] Without a colour for the nuclear star cluster, we note that the galaxy has $B_T - V_T = (12.19 - 0.101) - (11.72 - 0.077) = 0.446$, and $B_{F435W} - V_{F606W} = 0.446$ corresponds to $M/L_{F606W} = 0.98$ (Wilkins et al. 2013, their Eq. 2).

[12] http://rcsed.sai.msu.ru/catalog

[13] The primary target was NGC 4472 and its halo.

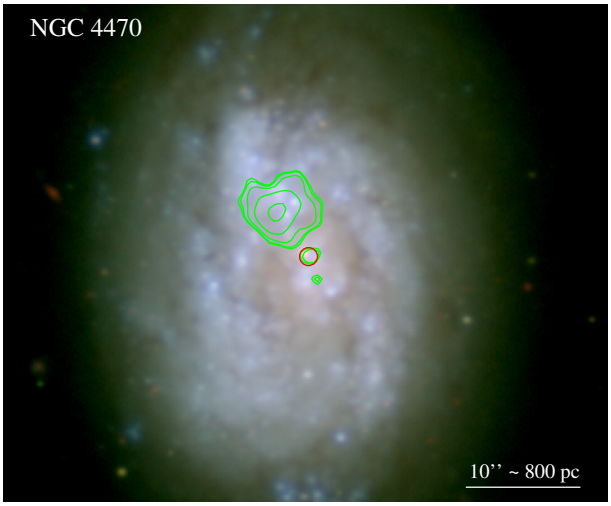

Figure 2. Next Generation Virgo Cluster Survey (NGVS: Ferrarese et al. 2012) image of NGC 4470 (red = i filter; green = g; blue = u^*), with *Chandra*/ACIS-S contours (0.5–7.0 keV band) overlaid in green. The contours are just a visual device to show the location of the X-ray source (accurate to ≈0″.6). North is up, east is to the left. The red circle shows the NED-provided position for the galaxy's optical nucleus, and it has a radius of 1″ in this and subsequent figures, roughly reflecting the associated uncertainty/range coming from different isophotes.

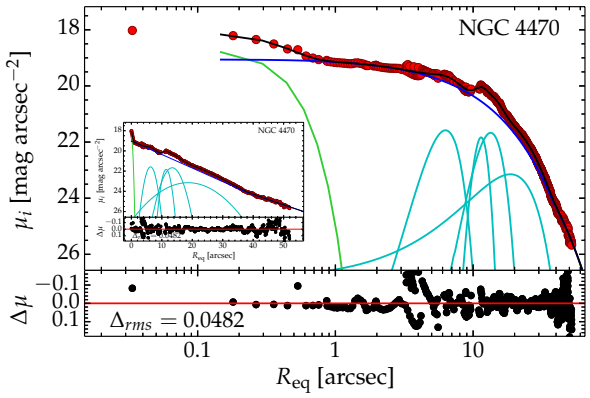

Figure 3. Similar to Figure 1, but for NGC 4470.

The galaxy's optical centre, as given by NED, coincides with a red feature which we could not resolve in the NGVS image with 0″.7 seeing. Figure 2 displays the over-lapping X-ray point-source at this central location. Both this X-ray source and the brighter source to the south proved too faint to acquire a spectrum.

Fitting a point-source to the i-band NGCS data, see Figure 3, yields a luminosity for the star cluster of $\log L_i/L_{\odot,i} = 6.57 \pm 0.35$. With an i-band mass-to-light ratio of 0.70±0.04, based on a galaxy $g-i$ colour equal to 0.69±0.03 and using the colour-dependent stellar mass-to-light ratios from Roediger & Courteau (2015), the corresponding stellar-mass of the nuclear star cluster is $\log M_{\rm nc}/M_{\odot} = 6.42 \pm 0.35$, and the predicted black hole mass is $\log M/M_{\odot} = 4.5 \pm 1.7$ (equation 1). However, this may be an upper limit due to contamination by AGN light increasing the light that we have assigned to the star cluster. That is, we have erred on the side of caution and are not under-predicting the IMBH mass. We also modelled the galaxy components in both the g- and i-band NGVS images, and we measured a $g-i$ colour equal to 0.57 for the nuclear component. This resulted in a 23% smaller stellar-mass estimate for the star cluster, and a 50% smaller estimate for the black hole mass. Although, this colour for the nuclear component may be influenced by AGN light and as such we have preferred the former measurement.

There is another equally bright source 2″.1 (170 pc) to the south, and a more extended source (∼10^{39} erg s^{-1}) located 6″ north-east of the nuclear position associated with an excess of blue stars and ongoing star formation. Based on the location of the second X-ray point-source, at 170 pc from the nucleus, it may be a stellar-mass, ultra-luminous X-ray binary (ULX: $L_X \approx 10^{39}$–10^{41} erg s^1), but is potentially more interesting than that if it represents one half of a dual IMBH system. A longer *CXO* exposure with the aim-point on NGC 4470 would enable this to be answered.

3.4 Galaxies with new X-ray data

3.4.1 NGC 4197: a likely bright IMBH

As with NGC 4178 above, NGC 4197 appears in the flat galaxy catalog of Karachentsev et al. (1993) due to the somewhat edge-on (inclination = 79 degrees) orientation of its disk relative to our line-of-sight. Dahari (1985) have reported weak H_α emission coming from the nucleus of this galaxy.

As a part of our Virgo cluster X-ray survey, NGC 4197 was observed by *CXO* for ≈8 ks, on 2017 July 26. We find a strong, point-like X-ray source (Figure 4) located at RA = $12^{\rm h}$ $14^{\rm m}$ $38^{\rm s}.59$, Dec = +05° 48′ 21″.2 [J2000.0]. Considering the scatter in the positions reported by NED, this is consistent with the position of the optical nucleus: it is ≈0″.7 (≈90 pc) away from the r-band SDSS position.

We extracted a spectrum within a 2″ circular source region (see Figure 5, with the local background extracted from the annulus between radii of 3″ and 9″. We then fit the spectrum in XSPEC, using the Cash statistics. We find that the spectrum (Figure 5) is well described (C-statistic of 62.7 for 50 degrees of freedom) by a power-law with photon index $\Gamma = 1.24^{+0.84}_{-0.69}$ and an intrinsic[14] column density $N_{\rm H} = 3.5^{+7.2}_{-3.5} \times 10^{21}$ cm^{-2}. The unabsorbed 0.5–7 keV flux is $F_{0.5-7\,{\rm keV}} = 1.1^{+0.3}_{-0.2} \times 10^{-13}$ erg cm^{-2} s^{-1}. After correcting for absorption according to our best-fitting power-law model, we derive a luminosity $L_{0.5-10\,{\rm keV}} = 1.4^{+0.7}_{-0.3} \times 10^{40}$ erg s^{-1}., at the assumed distance of 26.4 Mpc for this galaxy. If the X-ray spectrum corresponds to the low/hard state of an IMBH, the black hole mass would be $\gtrsim$ a few 10^3 solar masses.

We also tried to fit the spectrum with a disk-blackbody model. We rule out a peak disk temperature $T_{\rm in} \lesssim 1.6$ keV at the 90% confidence levels. Models with disk temperatures higher than that are acceptable (and, for $T_{\rm in} \gtrsim 3$ keV, essentially identical to the power-law model) because the peak

[14] By 'intrinsic', we are referring to the intervening number density beyond our Galaxy, primarily within the external galaxy.

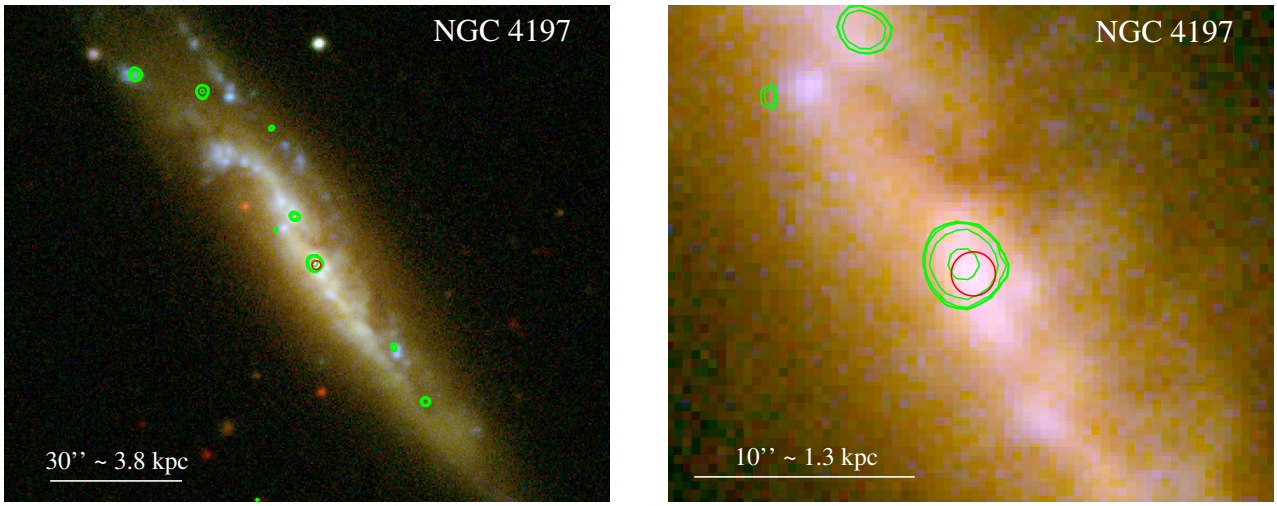

Figure 4. Left: Similar to Figure 2, but displaying a Sloan Digital Sky Survey (SDSS Alam et al. 2015) image of NGC 4197 (red = i' filter; green = g'; blue = u'). Right: Zoom-in on the inner region.

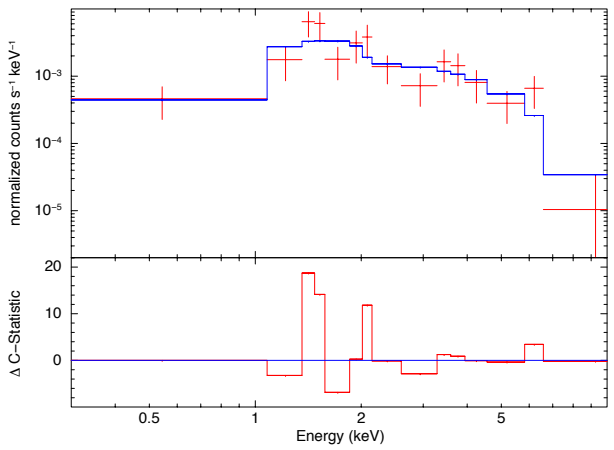

Figure 5. *CXO*/ACIS-S spectrum of the nuclear source in NGC 4197, fitted with a power-law model. The datapoints have been grouped to a signal-to-noise >1.8 for plotting purposes only. The fit was done on the individual counts, using Cash statistics. See Section 3.4.1 for the fit parameters.

emission moves close to or beyond the *Chandra* band, and we are only seeing the power-law-like section of the disk-blackbody below its peak. Disk temperatures of up to ∼2 keV are sometimes seen in stellar-mass ULXs with a super-critical disk (slim disk). Thus, we cannot rule out that the source is a $\approx 10^{40}$ erg s^{-1} stellar-mass ULX located exactly at the nuclear position, but the simplest explanation consistent with the data is that it is the nuclear BH of this galaxy.

The Eddington luminosity can be expressed as $L_{\rm Edd} \approx 1.26 \times 10^{38}\,(M_{\rm bh}/M_\odot)\,(\sigma/\sigma_{\rm T})^{-1}$ erg s^{-1}. Given that NGC 4197 has $L_{0.5-10\,{\rm keV}} = 144 \times 10^{38}$ erg s^{-1}, and assuming there is a hydrogen plasma with $\sigma = \sigma_{\rm T}$ (the Thomson scattering cross-section), this luminosity equates to a $\sim 10^2$ M$_\odot$ black hole accreting at the Eddington limit, or a ∼10 M$_\odot$ black hole accreting at ten times the Eddington limit. Alternatively, given that we have predicted $\overline{\log M_{\rm bh}} = 4.8 \pm 0.6$ for NGC 4197 (Table 1, the Eddington luminosity for such a black hole is $8.2^{+24.5}_{-6.1} \times 10^{42}$ erg s^{-1}. Expressing the Eddington ratio as $L_X/L_{\rm Edd}$, with $L_X \equiv L_{0.5-10\,{\rm keV}}$, implies an Eddington ratio of 0.0018, or 0.18 per cent. This is reasonably high, and as such one may expect the entire broadband emission from the nucleus to be dominated by the AGN (Falcke et al. 2004).

3.4.2 *NGC 4212: dual X-ray point sources 240 pc apart*

Decarli et al. (2007) report that NGC 4212 (aka NGC 4208) is a LINER/H$_{\rm II}$ composite galaxy. Filho et al. (2002, see their Table 1) searched for, but did not detect, a radio point-source in this galaxy which Sérsic (1973) noted had a peculiar amorphous nucleus, likely due to dust. Scarlata et al. (2004) report dust absorption almost down to the centre of the *HST* STIS *R*-band image, but they show a noticeable brightening within the core which is also evident in the NICMOS/F190N image from *HST* observing program 11080 (P.I.: D. Calzetti).

NGC 4212 is the only galaxy in our list of 15 spiral galaxies to have a predicted black hole mass greater than $\approx 10^5$ M$_\odot$, weighing in at $6^{+7}_{-3} \times 10^5$ M$_\odot$. However, it is particularly interesting and worthy of inclusion because we have discovered that there are *two* faint *CXO* sources near the nucleus, with one of them displaced by a little less than 1″ from the optical nucleus. Considering the positional uncertainty at such faint levels, and the presence of a dust lane likely shifting the optical centre northward, the X-ray point-source may be consistent with the optical nucleus.[15] The second, nearby, X-ray point-source is 2″.9 (≈240 pc) away. Their separation is resolvable with *CXO*, see Figure 6.

It is tempting to investigate the archived *HST* image of this galaxy in order to get at the galaxy's nuclear star cluster magnitude and mass. However, like the LINER/HII

[15] The X-ray point-source is too faint to establish whether or not it is moderately absorbed.

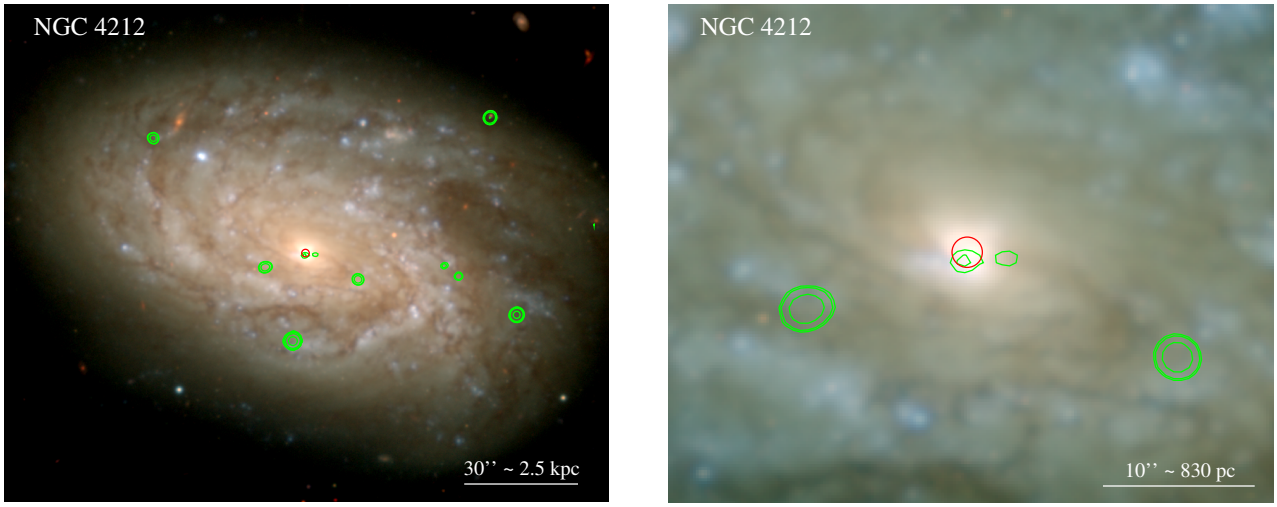

Figure 6. Similar to Figure 4, but displaying an NGVS image of NGC 4212.

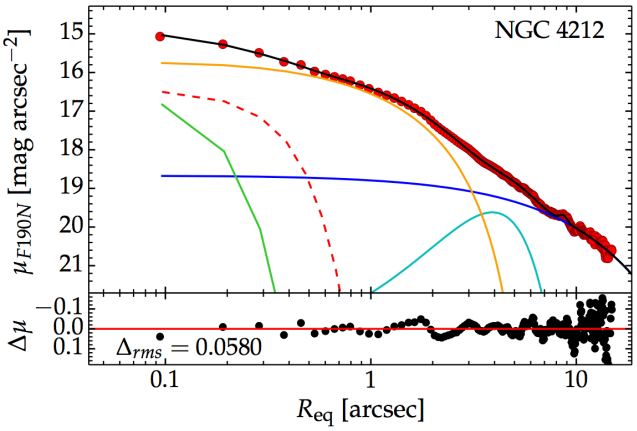

Figure 7. Similar to Figure 1, but for NGC 4212.

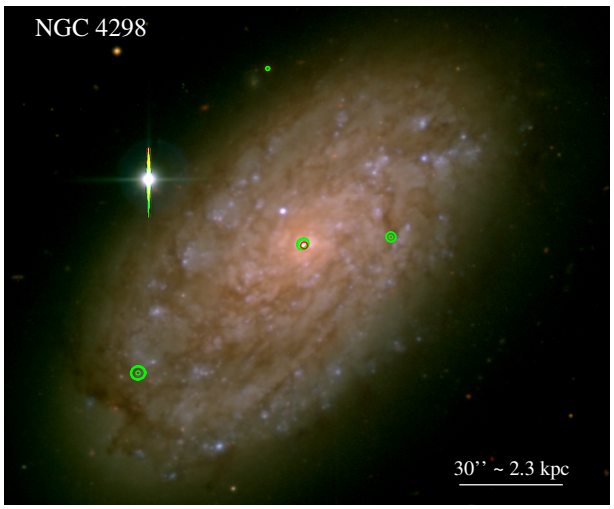

Figure 8. Similar to Figure 2, but displaying an NGVS image of NGC 4298.

galaxy NGC 4713, we need to be mindful that this is also a LINER/HII galaxy, and as such some of the excess nuclear light will be optical emission emanating from the unresolved, non-thermal AGN, as is the case in, for example, the LINER galaxy NGC 4486 (Ferrarese et al. 2006) and the Seyfert 1.5 galaxy NGC 4151 (Onken et al. 2014, see their Figure 4). Modelling the NICMOS/F190N image, we find the galaxy is well fit with a nuclear star cluster having a magnitude of 17.64±0.75 mag (AB) and a half-light radius of 0″.23 (19 pc), see Figure 7. For $M/L_{F190N} = 0.5 \pm 0.1$, this translates to a mass of $\log(M_{\rm nc}/M_{\odot}) = 7.05 \pm 0.34$, from which one would predict a black hole mass of $\log(M_{\rm bh}/M_{\odot}) = 6.2 \pm 1.6$, supportive of the expectation from the galaxy's stellar mass and spiral arm pitch angle (see Table 1).

3.4.3 NGC 4298

Figure 8 presents the optical and X-ray image for NGC 4298, while Figure 9 provides a decomposition of the galaxy light as seen in the WFC3/IR F160W image from *HST* observing program 14913 (P.I.: M. Mutchler).

Optical/near-IR nuclei in *HST* images may be active BHs and/or star clusters. Côté et al. (2006) showed that the nuclear star clusters in the Virgo cluster galaxies are slightly resolved with *HST/ACS*, enabling one to differentiate between point-sources and the spatially-extended star clusters. While the *HST's* spatial resolution is better in the UV and optical than it is in the infrared — simply because of how the diffraction limit scales linearly with wavelength — NGC 4298 is too dusty too see the nucleus at UV/optical wavelengths. However, NGC 4298 is clearly nucleated at 1.6 (and also 1.9) μm, and Figure 9 reveals that, using Profiler (Ciambur 2016), its nucleus can be well approximated by a Sérsic function (convolved with the *HST's* PSF) plus a tentative detection of a faint point-source. The Sérsic nucleus has a half-light radius equal to 0″.20 (15 pc) and an apparent (absolute) AB magnitude of 18.1±0.3 mag (−12.9±0.5 mag)

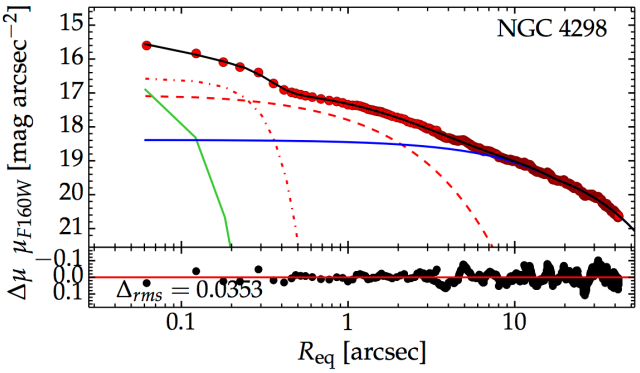

Figure 9. Similar to Figure 1, but for NGC 4298. The light is fit with a central point-source (green solid), a nuclear star cluster (red dot-dash), a bulge (red dash), and a truncated exponential disk (blue solid).

in the F160W band[16]. The tentative point-source, representing the putative AGN, has an apparent (absolute) magnitude of 20.4±0.3 mag (−10.6±0.5 mag).

Using an absolute magnitude for the Sun of $\mathfrak{M}_{\odot,F160W} = 4.60$ mag (AB) (Willmer 2018), and $M/L_{F160W} = 0.5$, gives a nuclear star cluster mass $\log(M_{\rm nc}/M_\odot) = 6.7 \pm 0.4$ and thus a predicted black hole mass of $\log(M_{\rm bh}/M_\odot) = 5.3 \pm 1.7$.

3.4.4 NGC 4313: dual X-ray point sources 590 pc apart

Decarli et al. (2007) report that NGC 4313 is a Seyfert/LINER galaxy. From our *CXO* data, we report the discovery of an apparently faint, point-like, X-ray source coincident[17] with the optical nucleus (Figure 10). Due to the galaxy's somewhat edge-on orientation, it may have a high intrinsic absorption of X-ray photons. Just one of the six X-ray photons is in the 0.3-1 keV band, 3 are in the 1-2 keV band, and 2 are in the 2-10 keV band. Offset by 8″.4 (590 pc) is a second, slightly fainter, X-ray point-source.

We have been able to inspect a NICMOS/F190N image from *HST* observing program: 11080 (P.I.: D. Calzetti) and decompose the galaxy light, which appears to consist of a bulge, plus a large-scale disk with a weak bar and ansae, and a nuclear star cluster with $m = 16.72 \pm 0.75$ mag, Sérsic $n \approx 0.8$ and $R_{\rm e} \approx 10$ pc (Figure 11). To obtain the mass of this nuclear component, we have used $\mathfrak{M}_{\odot,F190N} = 4.85$ mag (AB) (Willmer 2018), corrected for 0.011 mag of Galactic extinction, and assumed[18] $M/L_{F190N} = 0.5 \pm 0.1$. This yields a stellar-mass for the nuclear component of $\log M_{\rm nc} = 7.27 \pm 0.36$, and this value may be an underestimate given that there will be some internal extinction at 1.9 μm coming from within NGC 4313. This leads to a higher than anticipated black hole mass prediction of $\log M_{\rm nc} = 6.74 \pm 1.64$.

[16] Performing the decomposition without the point-source yields an apparent magnitude for the star cluster of 17.9±0.2 mag.
[17] As with NGC 4212, a dust lane has likely shifted the optical nucleus of NGC 4313.
[18] For reference, Barth et al. (2009) found a value of 0.47 for the nucleus of the late-type Sd galaxy NGC 3621.

3.4.5 NGC 4330: $L_X \approx 10^{40}$ erg s^{-1}

NGC 4330 is experiencing ram pressure stripping of both its neutral HI gas (Chung et al. 2007; Abramson et al. 2011) and its ionised gas (Vollmer et al. 2012; Fossati et al. 2018).

The edge-on orientation of its disk to our line-of-sight, coupled with the detection of a nuclear X-ray source, suggests that it may harbour an intrinsically bright AGN given that some X-rays have penetrated their way out through the disk plane (see Figure 12). For comparison, NGC 4197 and NGC 4313 (Figures 4 and 10) and NGC 4178 (GSD19) represent examples of spiral galaxies with *somewhat* edge-on disks in which we have detected a nuclear X-ray point-source.

In NGC 4330, the *CXO* source is ≈2″ from the optical centre reported by NED. However, as Figure 12 shows, the location of the dust lane, coupled with the slight banana shape of the galaxy, may result in the optical centroid derived from the outer isophotes not corresponding to the true nucleus of the galaxy, which might instead be flagged by the location of the *CXO* source. Among our sample of galaxies expected to possess a central IMBH, NGC 4330 has the second brightest central X-ray point-source after NGC 4197 (see Table 3).

As with NGC 4197, we were able to obtain a meaningful X-ray spectrum from the central point-source in NGC 4330 (see Figure 13). The background-subtracted spectrum was fit in XSPEC, using the Cash statistics, and well described by a power-law with a (fixed) photon index $\Gamma = 1.7$ and a high intrinsic column density of $N_{\rm H} = 4.3^{+2.9}_{-2.0} \times 10^{22}$ cm^{-2}. The unabsorbed flux $F_{0.5-7\,{\rm keV}} = 6^{+3}_{-2} \times 10^{-14}$ erg cm^{-2} s^{-1}. At a distance of 19.30 Mpc, this corresponds to a luminosity $L_{0.5-7\,{\rm keV}} = 1.727^{+0.645}_{-0.515} \times 10^{39}$ erg s^{-1}. Extrapolating the power-law, one has $L_{0.5-10\,{\rm keV}} = 0.9^{+0.6}_{-0.3} \times 10^{40}$ erg s^{-1}.

3.4.6 NGC 4492; dual X-ray point sources 550 pc apart

NGC 4492 is a new addition to the sample in GSD19, having useful *CXO* data from Cycle 8 (4.89 ks, Proposal 08700652, P.I.: S.Mathur) and Cycle 15 (29.68 ks, Proposal 15400260, P.I.: T.Maccarone), and an expected IMBH at its centre based upon the galaxy's stellar luminosity (see Table 1). Decarli et al. (2007) classified this galaxy as having no (H_α nor [NII]) emission lines based upon their 2″-slit spectra from the Bologna Faint Object Spectrograph (BFOSC) attached to the Loiano 1.5 m telescope. However, we find that it possesses a central X-ray point-source, and a second X-ray point-source 550 pc to the east of the nuclear point-source (Figure 14).

We have combined the above two *CXO* exposures (using the CIAO task *specextract*, with the option 'combine_spectra = yes') to obtain the spectrum of the faint nuclear source in NGC 4492. Figure 15 reveals a power-law spectral energy distribution (SED), with $\Gamma = 1.7$, as opposed to the blackbody radiation curve of a hot accretion disk.

After fitting the combined spectrum, we fixed $N_{\rm H}$ and Γ, leaving the normalisation parameter free, and fitted the two individual spectra in XSPEC. This yielded an observed nuclear flux of $F_{0.5-7\,{\rm keV}} = 1.2^{+0.8}_{-0.6} \times 10^{-14}$ erg cm^{-2} s^{-1} and $0.84^{+0.46}_{-0.34} \times 10^{-14}$ erg cm^{-2} s^{-1}, and a corrected luminosity of $L_{0.5-7\ {\rm keV}} = 6.6^{+4.3}_{-3.0} \times 10^{38}$ erg s^{-1} (in 2007) and $L_{0.5-7\ {\rm keV}} = 4.0^{+2.3}_{-1.6} \times 10^{38}$ erg s^{-1} (in 2014), with a 90 per cent confidence. Extrapolating slightly, this corresponds to

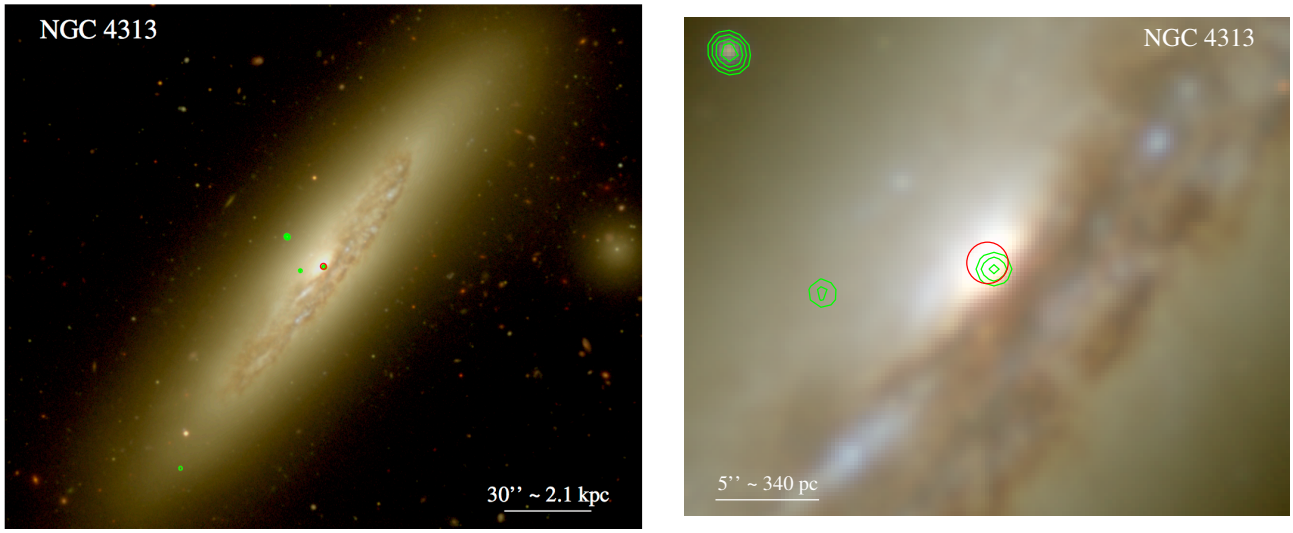

Figure 10. Similar to Figure 4, but displaying an NGVS image of NGC 4313.

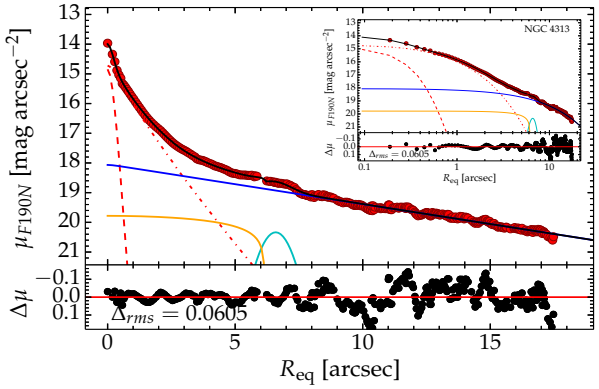

Figure 11. Similar to Figure 1, but for NGC 4313.

$L_{0.3-10\,\mathrm{keV}} = 7.2^{+5.0}_{-3.5} \times 10^{38}$ erg s^{-1} and $5.0^{+2.7}_{-2.0} \times 10^{38}$ erg s^{-1} for the ≈5 ks and ≈30 ks exposures, respectively.

3.4.7 NGC 4498

NGC 4498 contains a few knots of star formation along its spine, as seen in *HST* observing program 5446 (P.I.: G. D. Illingworth, WFPC2/F606W). As noted in Section 2, Georgiev et al. (2016) have reported a stellar-mass for the central star cluster of $(136^{+46}_{-41}) \times 10^4\,\mathrm{M}_\odot$ using a V-band mass-to-light ratio of $0.63^{+0.21}_{-0.19}$. Associated with this, we report the discovery of an X-ray point-source (Figure 14).

3.4.8 NGC 4519

Globally, like NGC 4713, NGC 4519 (Figure 14) somewhat resembles the barred, bulgeless spiral galaxy LEDA 87300. Centrally, NGC 4519 contains knots of star formation near its nucleus, and defining a single nuclear star cluster may prove problematic as there are multiple candidates seen in the *HST* images from observing program 9042 (P.I.: S.J.Smartt, F814W) and observing program 10829 (P.I: P.Martini, F606W).

3.4.9 NGC 4607: $L_X \approx 0.6 \times 10^{40}$ erg s^{-1}

As with the edge-on galaxy NGC 4330, NGC 4607 is also aligned edge-on to our line-of-sight. Given the expectedly high line-of-sight column density of neutral hydrogen through the disk of this galaxy, our discovery of a central X-ray source (Figure 14) suggests that it must be intrinsically bright and contain X-ray photons in the higher energy bands. While the central X-ray point-source has only a few counts, they all have energies above 1 keV, which suggests that the absorption intrinsic to NGC 4607, $\mathrm{N_{H,intrin}}$, is quite high. It also disfavours an XRB that is both in the outskirts of this galaxy and coincidentally lined up with our sight-line to the centre of this galaxy. Moreover, Decarli et al. (2007) have reported that NGC 4607 is a known LINER.

We constructed the X-ray spectrum using the CIAO task *specextract*, before regrouping the spectra to 1 count per bin prior to the Cash statistics analysis in XSPEC using a fixed power-law slope $\Gamma = 1.7$ and a free $\mathrm{N_{H,intrin}}$. The spectrum is shown in Figure 16. Although ratty, we wish to point out the grouping of counts around 6.4 keV. Although it could be due to the randomness of small-number statistics, it is more likely due to a strong Fe K_α fluorescence line (and a Compton reflection bump above 10 keV) from cold, near-neutral, material (disk, torus or clouds) irradiated by the nuclear X-ray source (Pounds et al. 1990). We hope to acquire a longer Chandra, or a new *NuSTAR*, observation in the future, also enabling a better constraint on the slope of the X-ray SED.

3.4.10 NGC 4405 & NGC 4413

With only 6 X-ray photons detected from the central X-ray source in NGC 4405 (see Figure 17), we consider it to probably be a point-source rather than extended emission.

Similar to NGC 4405, there are only 6 X-ray photons

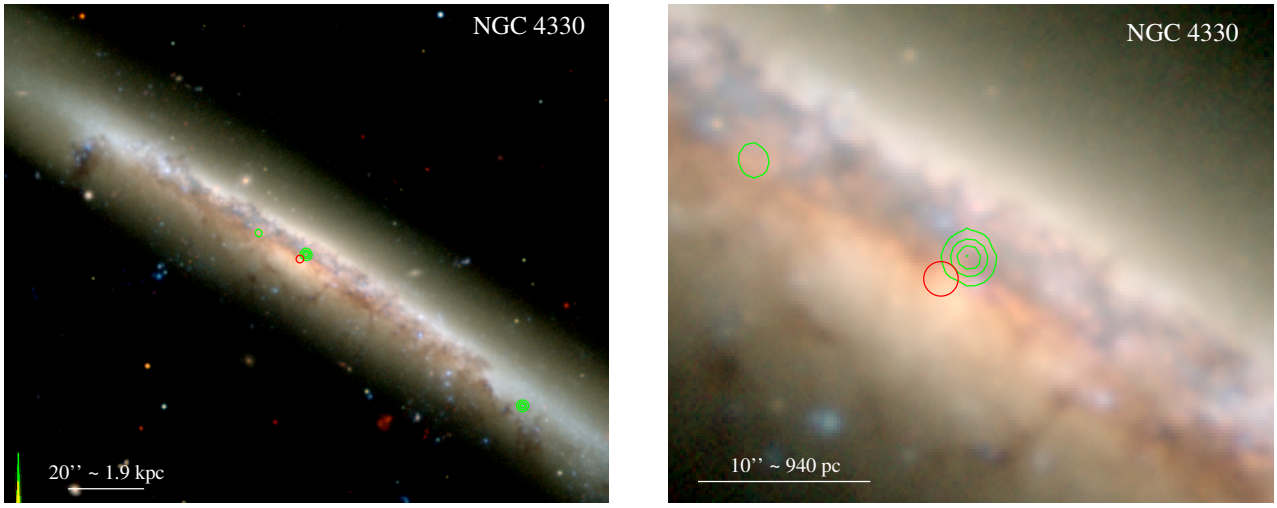

Figure 12. Similar to Figure 4, but displaying an NGVS image of NGC 4330.

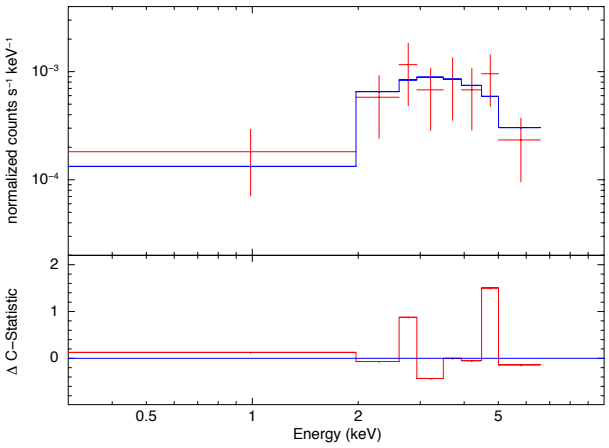

Figure 13. Similar to Figure 5, but for the edge-on galaxy NGC 4330, whose published optical centre may be displaced due to the intervening dust.

detected from the central X-ray source in NGC 4413 (aka NGC 4407, see Figure 17).

4 BLACK HOLE MASSES FROM THE X-RAY DATA

4.1 Point-sources with X-ray spectra

Although it is not yet feasible with the available X-ray data to distinguish between a stellar-mass and an IMBH/AGN, we outline two possible spectral clues that can be pursued via deeper *CXO* observations and/or with the proposed next generation of X-ray satellites including Athena (Nandra et al. 2013; Rau et al. 2013), AXIS (Mushotzky 2018), and Lynx (Gaskin et al. 2019).

The first distinction we address is between stellar-mass black holes and IMBHs. Standard accretion-state models predict that an IMBH or AGN at a luminosity of $\sim 10^{38}$–10^{39} erg s^{-1} should have an unbroken power-law spectrum in the 0.5-10 keV band (low/hard state), while a stellar-mass source (especially, a stellar-mass black hole) should have a disk-blackbody spectrum with a temperature $\sim$0.5–1 keV (high/soft state) and a normalization corresponding to characteristic radii $\sim$50–100 km. For example, this was the main argument in favour of the identification of the nuclear source in M33 ($\sim$20 times closer to us than the Virgo cluster) as a stellar-mass black hole (Foschini et al. 2004). There are, however, additional caveats in this simple classification. While transient stellar mass black holes near their Eddington luminosities can exhibit hard power law spectra in the hard intermediate state these phases are short-lived, typically lasting only a few days, and hence it is rather unlikely that a Chandra observation would catch a source in such a state (e.g. Homan & Belloni 2005; Motta et al. 2009). Moreover, neutron star X-ray binaries (X-ray pulsars) can also reach or exceed such luminosities, and at a moderate signal-to-noise ratio the Comptonized spectrum of those sources is also well approximated by a hard power-law, in the relatively narrow *Chandra* or *XMM-Newton* bands (Ferrigno et al. 2009; Farinelli et al. 2016; Pintore et al. 2017). The X-ray-to-optical flux ratio criterion is also inapplicable for nuclear sources, because in most cases we can only measure the optical brightness of the host star cluster, not the direct optical emission from the disk or the donor star of the X-ray source. As an indication of the difficulty of the task for galaxies in the Virgo cluster, one need only read the discussion about the nuclear black hole identification in the much closer M83 galaxy by Russell et al. (2020).

The second distinction, although likely an artificial one created out of observational selection bias, is between IMBHs (10^2–10^5 M$_\odot$) and SMBHs in the 10^6–10^7 M$_\odot$ mass range. In the X-ray luminosity range $\sim 10^{38}$–10^{39} erg s^{-1}, both an IMBH and a 'normal' SMBH, with say $M_{\rm bh} \sim 10^6\,M_\odot$, would be lumped together in the low/hard state, according to the traditional state classification. However, more recent studies of accreting BHs in this low-luminosity regime show further physical changes as a function of the Eddington ratio $L_{\rm Edd} \equiv L_{\rm bol}/L_{\rm Edd}$ ($\approx L_{\rm X}/L_{\rm Edd}$ for stellar-mass

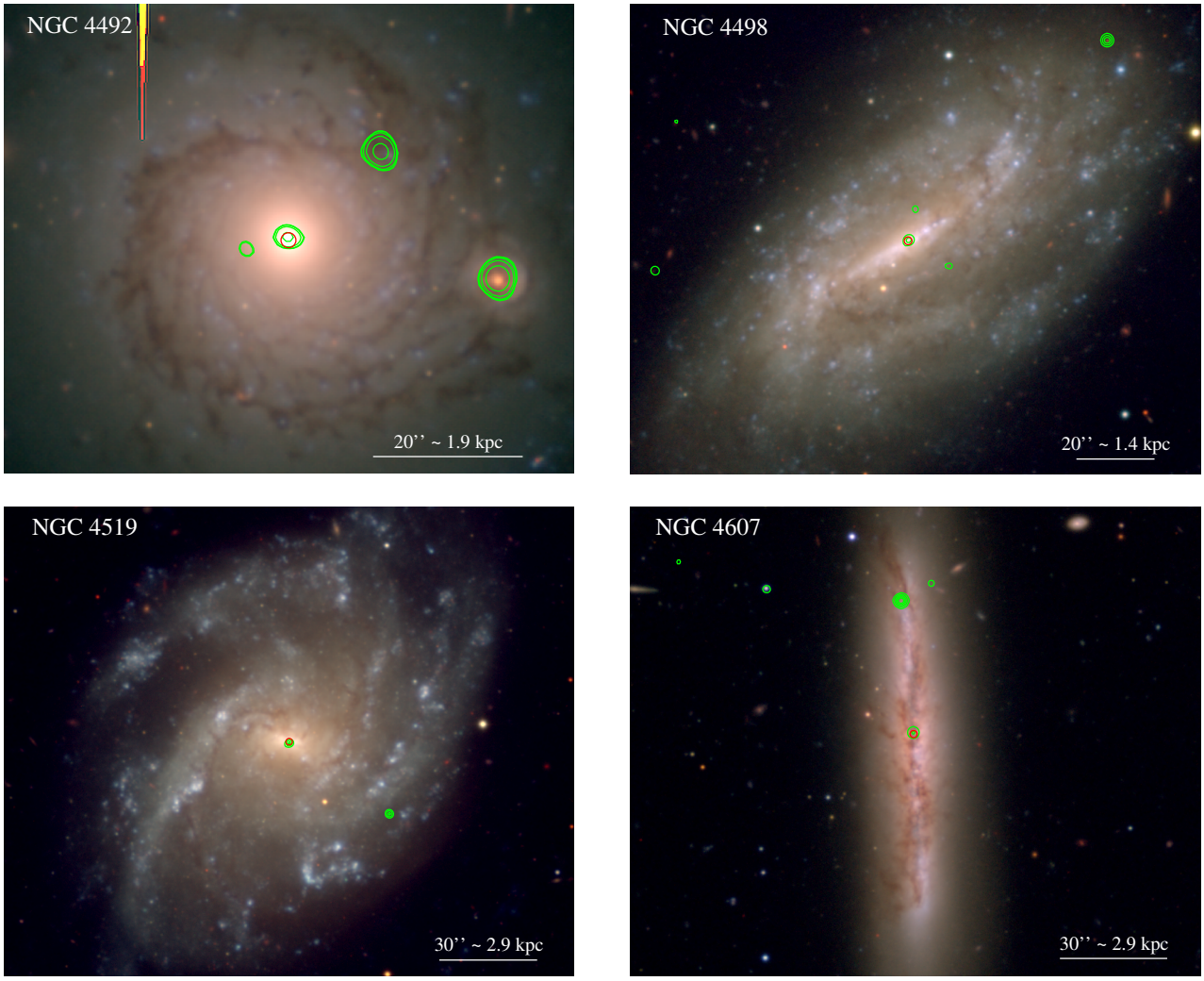

Figure 14. Similar to Figure 2, but displaying NGVS images of NGC 4498, NGC 4519, NGC 4492, and NGC 4607. For NGC 4492, the bright source to the right is the nucleus of the galaxy SDSS J123057.82+080434.7 (Wang et al. 2016), and the red/yellow bleed is from a bright adjacent star.

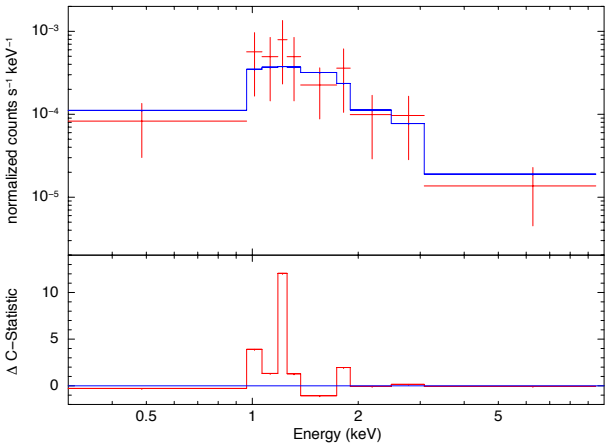

Figure 15. Similar to Figure 5, but for NGC 4492.

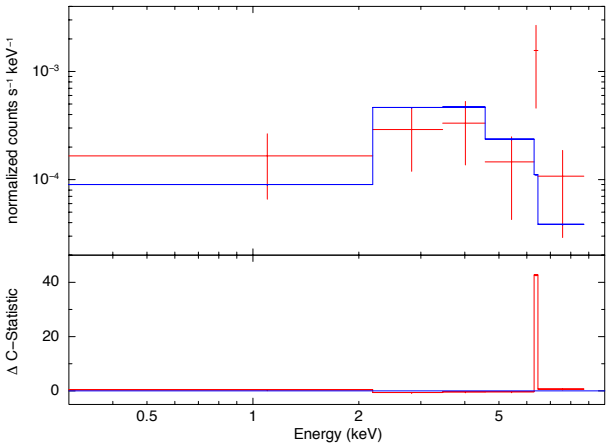

Figure 16. Similar to Figure 5, but for NGC 4607.

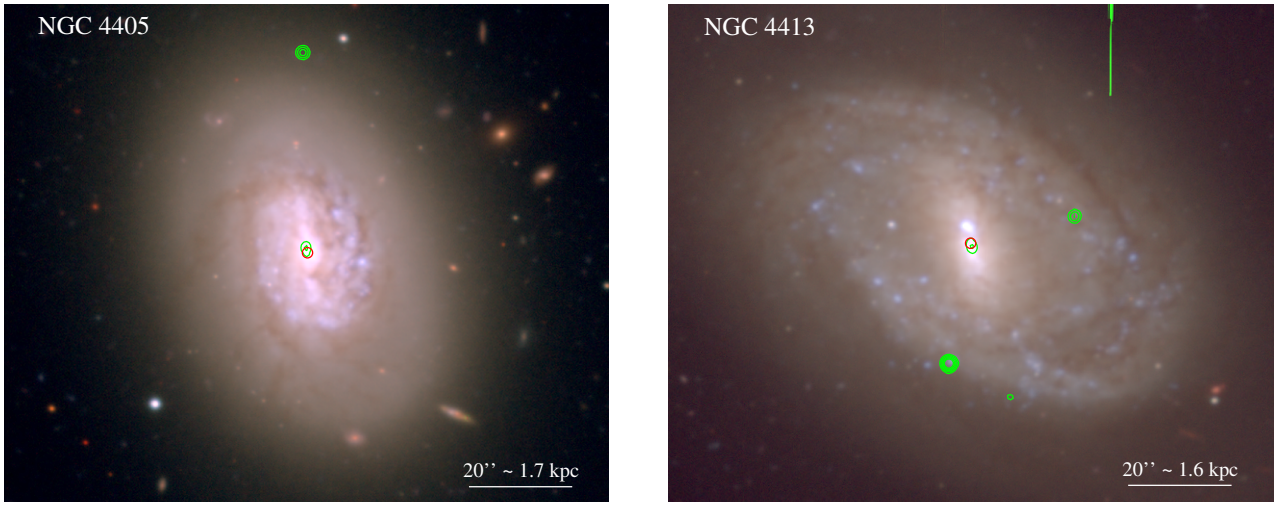

Figure 17. Similar to Figure 2, but displaying NGVS images of NGC 4405 and NGC 4413 (aka NGC 4407). For these two galaxies, the central X-ray photon count was low, and as such we *tentatively* consider them to be X-ray point-sources.

BHs). The hardest spectra ($\Gamma \approx 1.7$) occur at $L_{\rm Edd} \sim 10^{-3}$; below that threshold, the X-ray spectrum progressively softens again, reaching an asymptotic value of $\Gamma \approx 2.1$ at $L_{\rm Edd} \sim 10^{-5}$ and below (Sobolewska et al. 2011; Armas Padilla et al. 2013; Plotkin et al. 2013; Yang et al. 2015; Plotkin et al. 2017). For example, a SMBH with $M_{\rm bh}$ around a few $10^6\,M_\odot$ and $L_{\rm X} \approx$ a few 10^{38} erg s^{-1} will have an Eddington ratio $L_{\rm Edd} \sim 10^{-5}$ (assuming a bolometric correction $L_{\rm bol}/L_{\rm X} \approx 10$: Lusso et al. 2012). Instead, an IMBH at the same X-ray luminosity may have $L_{\rm Edd} \sim 10^{-3}$. Thus, a low-state IMBH should have a moderately harder spectrum than a more massive nuclear BH, at the same X-ray luminosity. We suggest that for a sufficiently high signal-to-noise ratio in the X-ray spectra, it will be possible to discriminate between the two cases: if not for individual sources, at least based on the statistical distribution of fitted photon indices.

4.2 Fundamental Plane of black hole activity

The "fundamental plane of black hole activity" for black holes with low accretion rates (Merloni et al. 2003; Falcke et al. 2004; Fischer et al. 2020) encompasses stellar-mass black hole X-ray binaries and AGN, and enables one to estimate the black hole mass based upon the nuclear radio emission, $L_R = \nu L_\nu$ erg s^{-1} (at 5 GHz), and the unabsorbed nuclear X-ray luminosity, L_X erg s^{-1} (at 0.5-10 keV). Plotkin et al. (2012) report the following correlation

$$\log L_X = (1.45\pm0.04)\log L_R - (0.88\pm0.06)\log M_{\rm bh} - (6.07\pm1.10). \quad (5)$$

For $M_{\rm bh} = 10^5\,{\rm M}_\odot$ and $L_X = 10^{40}$ erg s^{-1}, one obtains an expected radio luminosity νL_ν(5 GHz) of $10^{34.8}$ erg s^{-1}, while for $M_{\rm bh} = 3\times10^3\,{\rm M}_\odot$ and $L_X = 10^{38}$ erg s^{-1}, one obtains an expected radio luminosity νL_ν(5 GHz) of $10^{32.5}$ erg s^{-1}. At an average distance of 17 Mpc, this corresponds to 0.04 mJy and 0.18 μJy, respectively. Using the correlation from Gültekin et al. (2019), which is based on the 2-10 keV luminosity[19], these estimates are 0.03 mJy and 0.08 μJy. This latter value is ∼7 times smaller than the estimate of 0.54 μJy obtained using the correlation from Gültekin et al. (2009). For reference, Strader et al. (2012) searched for radio emission from potential IMBHs in three globular clusters but found no source down to rms noise levels of 1.5–2.1 μJy beam^{-1} with the Very Large Array (VLA). Tremou et al. (2018) have also reported a non-detection of IMBHs with $M_{\rm bh} \gtrsim 10^3$ M$_\odot$ (3σ) in globular clusters, with a VLA image stack of 24 GCs having an rms sensitivity of 0.65 μJy beam^{-1}, and an ACTA image stack of 14 GCs having an rms sensitivity of 1.42 μJy beam^{-1}. It will, however, be interesting to explore the Andromeda Galaxy's very low metalicity globuar cluster RBC EXT8 (Larsen et al. 2020) — taken from the Revised Bologna Catalogue (Galleti et al. 2004) — which may have formed more massive stars than is usual (see also Wan et al. 2020, in regard to the Phoenix stream/GC).

Reversing the above argument, one can use X-ray luminosities with radio observations to predict the black hole masses, or at least obtain an upper limit if only upper limits to the radio luminosity of any compact nuclear sources exist. We scanned the literature for radio data, and found one observation. With 0″.15 spatial resolution, Nagar et al. (2005) reported an upper limit to the nuclear flux in NGC 4713 of ≈1.10 mJy at 15 GHz (2 cm), or $\log(L_{\nu,15\ GHz}\,W\,Hz^{-1}) < 19.63$ for $D = 17.9$ Mpc. This equates to $\log(\nu\,L_{\nu,15\ GHz}\,{\rm erg\,s^{-1}}) < 36.81$. However, we do not know the slope of the radio SED, required to obtain the luminosity at 5 GHz. Moreover, given the available X-ray flux and anticipated black hole mass in NGC 4713, one requires constraints on the radio flux which are some three orders of magnitude tighter, at around 1 μJy. Furthermore, Nagar et al. (2005) report significant inter-year variability at 15 GHz and, for a given black hole, the radio and X-ray flux are correlated (Hannikainen et al. 1998; Brocksopp et al. 1999; Corbel et al. 2003).

Capetti et al. (2009) obtained VLA images for 63 of

[19] For $\Gamma = 1.7$, $L_{2-10\,\rm keV} = 0.646 L_{0.5-10\,\rm keV}$.

the 100 early-type galaxies in the Virgo Cluster compiled by Côté et al. (2004), but they detected compact radio sources at the centres of just 12 of these (with fluxes from 0.13 mJy to 2.7 Jy), and no compact radio cores in any of the 30 lowest mass galaxies with $M_{*,\rm gal} < 1.7 \times 10^{10}\,M_\odot$. In GSD19, we reported that only 3 of the 30 galaxies (from the larger set of 100) that were expected to have a central IMBH also had a central X-ray point-source. However, for our sample of 75 spiral galaxies with ongoing star-formation, and thus cold gas to potentially fuel a greater level of accretion onto a central IMBH, we have found that, excluding NGC 4178) 13 of the 33 galaxies expected to have an IMBH also have a X-ray point source in their centre. As such, there is hope for detecting the brighter sources in our sample at radio wavelengths, and the large collecting area of radio facilities with the spatial resolution to detect compact radio sources, such as the VLA, the next generation Very Large Array (ngVLA Carilli et al. 2015), and the upcoming Square Kilometer Array radio telescope (SKA: Dewdney et al. 2009), will play a key role in detecting the fainter sources.

5 DISCUSSION

5.1 Chasing the sphere-of-influence

It is regularly speculated that dwarf galaxies may contain relic seed black holes from the early Universe. If the dwarf galaxy is itself a relic, then this may be correct, but if the dwarf galaxy has experienced accretion, mergers, star formation and AGN activity since its presumed monolothic collapse, then it is plausible, if not likely, that the central black hole is no longer a relic seed, but something more massive. It is noted that the relic seeds may be 300 to 10^4 $\rm M_\odot$ (Bond et al. 1984; Carr et al. 1984; Regan et al. 2020), rather than the 10^5 $\rm M_\odot$ black holes often used in simulations. Given the ongoing growth of some dwarf galaxies, the IMBHs observed in them would be suggestive of (at least some of the) black hole seeds having yet smaller masses.

From our parent sample of 74+1 late-type galaxies in the Virgo cluster, only three (NGC: 4303, 4388, and 4501)[20] have had directly measured black hole masses reported (see Table A2 in GSD19). While two of these are reported to have black hole masses greater than $\sim 10^7\,\rm M_\odot$, NGC 4303 ($D \approx$ 12-13 Mpc, $\sigma = 95$ km s^{-1}) has the smallest reported black hole mass of the three, at $4 \times 10^6\,\rm M_\odot$ (Pastorini et al. 2007, observed with *HST*/STIS). For reference, from the sister sample of 100 early-type galaxies in the Virgo cluster (Côté et al. 2004) that were also observed with *CXO* (Gallo et al. 2008), there are the 11 galaxies which currently have directly measured black hole masses (see Table 1 in Graham & Soria 2019), and all but one of those[21] have black hole masses greater than $\sim 2 \times 10^7\,\rm M_\odot$.

Table 2. Black hole calibration points

$M_{\rm bh}$ $\rm M_\odot$	σ km s^{-1}	$r_{\rm soi}$ pc ($''$)
10^9	293	50 (0.6)
10^8	195	11.3 (0.14)
10^7	130	2.5 (0.03)
10^6	86	0.6 (0.007)
10^5	57	0.13 (1.6E-3)
10^4	38	0.03 (3.6E-4)
10^3	25	0.007 (8.3E-5)
10^2	17	0.001 (1.8E-5)

Reversing the spiral galaxy $M_{\rm bh}$–σ bisector relation (Davis et al. 2017, their Table 4 entry "All") we provide both the stellar velocity dispersion that corresponds to the black hole masses listed in column 1, and the expected sphere-of-influence (soi) of the black hole if at a typical Virgo cluster distance of 17 Mpc.

Table 2 reveals the typical spatial resolution required to resolve the gravitational sphere-of-influence (soi) around black holes of different mass and located at a typical Virgo cluster distance of 17 Mpc. These estimates are based upon the expression $r_{\rm soi} = GM_{\rm bh}/\sigma^2$ (Peebles 1972; Frank & Rees 1976), which is informatively reviewed in Merritt & Ferrarese (2001) and Merritt (2013). Obviously for local galaxies, if they are half this assumed distance then their apparent $r_{\rm soi}$ (in arcsec, not in parsec) will double.

It is pertinent to ask, and interesting to know, what prospects there are for high(er) spatial resolution observations. In space, the 6.5m James Webb Space Telescope (*JWST*) will hopefully soon accompany the 2.4m *HST*, with NIRCam (Horner & Rieke 2004) aboard *JWST* providing a diffraction-limited spatial resolution of ≈70 milliarcseconds (mas), as defined by the PSF's FWHM at 2 microns. This is comparable to the angular resolution achieved at UV wavelengths with *HST's* long-slit Space Telescope Imaging Spectrograph (STIS: Woodgate et al. 1998). Building on the 8-10m class optical/near-IR telescopes with adaptive optics, such as the Very Large Telescope[22] (*VLT*), the Keck twin telescopes, and the Gran Telescopio Canarias (*GTC*), there are the upcoming 20-40m class telescopes, with the 24.5m Giant Magellan Telescope (*GMT*) expected to have a diffraction-limited resolution of ∼13 mas in the *J*-band (∼22 mas in the *K*-band) feeding the *GMT* integral field spectrograph (GMTIFS: McGregor et al. 2012), while the Thirty Meter Telescope (*TMT*) boasts 4 mas spaxels and 8 mas resolution from its Infrared Imaging Spectrograph (IRIS: Larkin et al. 2016). The 40m European Extremely Large Telescope (*E-ELT*) will be equipped with the High Angular Resolution Monolithic Optical and Near-Infrared (HARMONI: Thatte et al. 2016) integral field spectrograph,

[20] The recent compilation of directly measured black hole masses given by Sahu et al. (2019b) reports two additional late-type galaxies, with directly measured black hole masses, in/near the Virgo cluster. They are NGC 4151 (Gursky et al. 1971; Wood et al. 1984) with $M_{\rm bh} \sim 5 \times 10^7\,\rm M_\odot$, and NGC 4699 (González Delgado et al. 1997) which belongs to the NGC 4697 Group (Makarov & Karachentsev 2011) and has $M_{\rm bh} \sim 2 \times 10^8\,\rm M_\odot$.

[21] NGC 4486A (VCC 1327, $D = 18.3$ Mpc, $\sigma = 131 \pm 13$ km s^{-1}) has the lowest reported black hole mass at $(1.3 \pm 0.8) \times 10^7\,\rm M_\odot$. It was observed with the integral field spectrograph SINFONI on the Very Large Telescope under $0''.1$ spatial resolution by Nowak et al. (2007).

[22] MAVIS will have 20 mas spatial resolution at 550 nm (McDermid et al. 2020).

also with 4×4 mas spaxels. This represents roughly an order of magnitude improvement, and will enable one to resolve the sphere-of-influence around Virgo cluster BHs of mass down to 10^6 $M_\odot$ (see Table 2). Impressively, the GRAVITY near-infrared interferometric instrument involving all four of the 8 m Very Large Telescopes (VLT) already provides 2-4 mas resolution (e.g., Collaboration et al. 2020).

For the 100+ galaxies within the Local Group that are more than ten times closer than the Virgo cluster's mean distance, i.e. within 1.7 Mpc, the *TMT* and *E-ELT* will be able to probe BHs that are some ten times smaller, encompassing the galaxies M33, NGC 185, NGC 205, NGC 300, NGC 147, NGC 3109, NGC 6822, IC 10, IC 1613, IC 5152, UGC 4879, DDO 216, DDO 210, DDO 221, Leo I, II & III, Sextans A & B, Antlia, etc. One will even be able to probe down to black hole masses of 10^4 $M_\odot$ if they are within 170 kpc, encompassing the many satellites of the Milky Way, such as the Magellanic Clouds 50 and 63 kpc away, Sextans, Ursa Minor, Draco, Fornax, Sculptor, Carina, Pisces I, Crater II, Antlia 2, etc. Although, for BHs with a mass of 10^4 $M_\odot$ and a soi equal to 0.03 pc, if the host system has a velocity dispersion of 38 km s^{-1}, the number of stars within the soi may be limited. The soi around possible IMBHs within the Galaxy (see Oka et al. 2017; Ravi et al. 2018), out to distances of 17 kpc, could be resolvable for masses down to 10^3 $M_\odot$.

Considering facilities with longer baselines, ALMA, with its 16 km baseline, already provides 20 mas resolution at 230 GHz (1.3 mm), several times better than current optical/near-IR telescopes. Of course, it must be noted that observations by Miyoshi et al. (1995) of maser emission from a circumnuclear disk in NGC 4258 (M106) were made using a synthesized beam size of just 0.6×0.3 mas, obtained using 22 GHz (1.3 cm) interferometry on the Very Long Baseline Array (VLBA).[23] Indeed, this enabled confirmation that BHs are real, as opposed to say a swarm of compact stellar-mass remnants. Not surprisingly, this result led to searches for more such maser detections around BHs, and quite a few discoveries were made (e.g. Greenhill et al. 2003; Kuo et al. 2011; Humphreys et al. 2016). Emissions at the above mentioned radio/mm wavelengths do however stem from gas rather than stars. This can be problematic due to non-gravitational motions. As such, one does need to be mindful/hopeful of finding gas clouds in stable orbital configurations, which is not always the case — hence the preference for stellar kinematics much of the time. Most dramatically, recent observations at 1.3 mm wavelengths with the *Event Horizon Telescope* (*EHT*) have provided the highest resolution images to date. With 20 μas resolution, The Event Horizon Telescope Collaboration et al. (2019) probed not just within the soi, but were able to see the silhouette of the event horizon around the SMBH in M87, located ∼17 Mpc away in the Virgo cluster. Such spatial resolution also matches the soi of a 100 solar mass black hole 17 Mpc away (see Table 2), although the radio flux from such a source may not be high enough for the *EHT*.

[23] The VLBA can now achieve 0.12 mas (120 μas) resolution at a wavelength of 3 mm, using the MK-NL baseline, and the ngVLA may spatially resolve SMBH binaries and triples (Burke-Spolaor et al. 2018).

5.2 Future work/observations

There are several followup observations and investigations which would yield greater information and insight. For example, it would be of interest to uncover, through longer X-ray exposures, additional power-law spectra like we have found for NGC 4197. In a follow-up paper, we intend to present a detailed analysis of this target, combining multiple black hole mass estimates from a wide array of independent methods. Such an approach was used with the spiral galaxy NGC 3319, which has a centrally-located X-ray point-source, and which initially had a black hole mass estimate of $3{\times}10^2$–3×10^5 $M_\odot$ based on an assumed Eddington ratio of 0.001–1 (Jiang et al. 2018), but for whom an error-weighted meta-analysis of nine independent estimates yielded $M_{\rm bh} = (2.3^{+5.3}_{-1.6}) \times 10^4$ $M_\odot$ (Davis & Graham 2020).

Longer *CXO* exposures, plus *NuSTAR* and *XMM-Newton* exposures if its larger PSF does not encounter 'crowding' issues and the source count is high enough to overcome the larger background level, on interesting targets would also be of benefit. This would enable the X-ray spectral energy distribution (SED) modelling of the high-energy X-ray photons coming from hot accretion discs, and/or Compton scattering in a hot inflow, or inverse Compton emission from the magnetically-powered jet base or corona above the disk, and/or synchrotron X-ray emission related to the unobscured part of an inner jet (e.g. Pringle & Rees 1972; Narayan & Yi 1995; Tzanavaris & Georgantopoulos 2007). Longer X-ray exposures for NGC 4212 would be valuable for establishing, through higher quality spectra, the existence of a possible dual AGN, similar to the pair in NGC 6240 (Komossa et al. 2003; Fabbiano et al. 2020) but with a separation of ∼240 pc rather than 1 kpc. NGC 4470, NGC 4492 and NGC 4313, with their X-ray point-source separations of 170, 550 and 590 pc, respectively, could also be checked.

The large collecting area of the upcoming ngVLA and SKA, plus the Five-hundred-meter Aperture Spherical radio Telescope (*FAST*, aka Tianyan: Nan 2006; Li et al. 2013), and the current SKA pathfinder MeerKAT (originally the Karoo Array Telescope: Booth et al. 2009; Jonas 2009), and the Low-Frequency Array (LOFAR: van Haarlem et al. 2013) should prove valuable for detecting faint radio sources. Coupled with the improved spatial resolution from long-baseline interferometry, we hope to search for masers around IMBHs (e.g. Green et al. 2015) and probe the immediate vicinity of the AGN and the base of their jets (Tingay et al. 2000; Hough et al. 2002; Paragi et al. 2015; Doi et al. 2013).

In addition to the 'fundamental plane of black hole activity' (Merloni et al. 2003; Falcke et al. 2004; Dong & Wu 2015; Liu et al. 2016; Nisbet & Best 2016), which is used to estimate the mass of a black hole, alternative estimates come from indirect measurements, involving observable quantities which do not directly prove the existence of a Keplerian velocity profile around the black hole. While reverberation mapping of AGN can probe the gas clouds within the BH's sphere-of-influence, the assumptions about the orbital stability (virialised nature) and geometry of these clouds, coupled with the use of a mean virial f-factor to convert virial products, $r\Delta V^2/G$, into virial masses (e.g. Bahcall et al. 1972; Peterson & Wandel 2000), can hinder confidence in the estimated black hole mass. In application, the virial factor is currently assumed to be constant for all AGN, and

for IMBHs it is further based upon the assumption that this constant value can be extrapolated to masses less than 10^6 $M_\odot$, i.e. masses used to establish its value (e.g. Peterson et al. 2004; Graham et al. 2011). However, on a more reassuring note, while the presence of high-ionisation optical emission lines supports the presence of a black hole (Baldwin et al. 1981; Veilleux & Osterbrock 1987; Kewley et al. 2006; Martínez-Palomera et al. 2020; Mezcua & Domínguez Sánchez 2020), the presence of Doppler-broadened gas emission lines — used in calculating the virial product under the assumption that the broadening traces the velocity dispersion due to virialised motions around the black hole, as opposed to non virialised motion or outflows (e.g. Manzano-King et al. 2019, see their Appendix A) — do imply the presence of an IMBH rather than a stellar-mass black hole. We therefore intend to pursue the acquisition of Keck spectra to search for such emission lines in the Virgo cluster galaxies, enabling us to potentially derive a virial mass for the X-ray detected black holes.

The Kamioka Gravitational Wave Detector (*KAGRA*: Aso et al. 2013), with its 3 km baseline, and the famous *LIGO/VIRGO* facilities (Abramovici et al. 1992; Caron et al. 1997; Harry & LIGO Scientific Collaboration 2010; Acernese et al. 2015), are constrained to detect the collision of BHs less massive than ∼200 $M_\odot$. Thus far, *LIGO/VIRGO* have reported a bounty of BHs with masses tens of times the mass of our Sun, along with the collisional-creation of a black hole with mass equal to 98^{+17}_{-11} $M_\odot$ (Zackay et al. 2019) and 142^{+28}_{-16} $M_\odot$ (The LIGO Scientific Collaboration et al. 2020). The proposed underground Einstein Telescope (ET: Punturo et al. 2010; Gair et al. 2011; Huerta & Gair 2011) is planning to have a 10 km baseline with detector sensitivities that should enable it to detect IMBHs across the Universe, as will the planned Cosmic Explorer (CE: Reitze et al. 2019) with its 40 km baseline. It is anticipated that the planned Deci-Hertz Interferometer Gravitational wave Observatory (*DECIGO*: Kawamura et al. 2011), and the European Laser Interferometer Space Antenna (*LISA*) Pathfinder mission[24] (Anza et al. 2005; McNamara et al. 2013) will also help to fill the relative void between ∼10^2 and ∼10^5 $M_\odot$. They will be capable of capturing oscillations in the fabric of spacetime due to extreme- and intermediate-mass ratio inspiral (EMRI and IMRI) events around IMBHs (Gair et al. 2004; Mapelli et al. 2012; Merritt 2015; Babak et al. 2017; Bonetti & Sesana 2020), and IMBH-IMBH mergers from dwarf galaxy collisions (Bekki & Chiba 2008; Yozin & Bekki 2012; Graham et al. 2012; Cloet-Osselaer et al. 2014; Paudel et al. 2018; Conselice et al. 2020; Zhang et al. 2020; Barausse & Lapi 2020).

6 SUMMARY

We have discovered central, or close to central, X-ray point-sources in eleven Virgo cluster spiral galaxies expected to harbour an IMBH. This adds to the three already known in the literature: NGC 4713 Terashima et al. (2015), NGC 4178 Secrest et al. (2012), and NGC 4470 (GSD19). Moreover, it represents nearly half of our sample of 33+1 spiral galaxies expected to possess an IMBH. This contrasts notably with the 10% (central X-ray point-source) detection rate in a sample of 30 Virgo cluster early-type galaxies expected to possess an IMBH (Graham & Soria 2019), even though both samples had comparable exposure times of typically more than a couple of hours per galaxy. We suggest that this outcome may not necessarily reflect the occupation fraction of IMBHs, but rather the Eddington ratios in these two samples: the spiral galaxies were selected on the basis of having a star-formation rate greater than ∼0.3 $M_\odot$ yr^{-1}. That is, the spiral galaxies had cool gas available, and this is a valuable clue for future observing campaigns pursuing AGN in low-mass and dwarf galaxies.

The AGN in NGC 4197, for which we predict M_{bh} = 6×10^4 $M_\odot$ (see Table 1), was sufficiently strong that we modelled its power-law X-ray spectrum, consistent with the low/hard state of a greater than stellar-mass black hole.

We have also detected a clear, dual X-ray point-source in NGC 4212, with the off-centre point-source located 2.9 arcsec (240 pc) away from the centrally-located source. a Further observation is required to establish if it is the first dual IMBH. We note that NGC 4470, NGC 4492 and NGC 4313 are also new targets of interest due to their (weaker) dual X-ray point-sources, with one of each pair of point-sources residing at the centre of each of these galaxies, and the partner 170, 550 and 590 pc distant.

ACKNOWLEDGEMENTS

Support for this work was provided by the National Aeronautics and Space Administration through Chandra Award Number LP18620568 issued by the Chandra X-ray Center, which is operated by the Smithsonian Astrophysical Observatory for and on behalf of the National Aeronautics Space Administration under contract NAS8-03060. This research was supported under the Australian Research Council's funding scheme DP17012923, and by the French Centre National d'Etudes Spatiales (CNES). This material is based upon work supported by Tamkeen under the NYU Abu Dhabi Research Institute grant CAP^3. Part of this research was conducted within the Australian Research Council's Centre of Excellence for Gravitational Wave Discovery (OzGrav), through project number CE170100004.

7 DATA AVAILABILITY

The data underlying this article are available in the Chandra Data Archive (CDA: https://cxc.harvard.edu/cda/), the Sloan Digital Sky Survey archive (http://skyserver.sdss.org/), the Next Generation Virgo Cluster Survey website (https://www.cfht.hawaii.edu/Science/NGVS/), the Hubble Space Telescope section of the Mikulski Archive for Space Telescopes (MAST: https://archive.stsci.edu/hst/), the NASA/IPAC Extragalactic Database (NED: http://nedwww.ipac.caltech.edu), the HyperLeda database (http://leda.univ-lyon1.fr), the GOLD Mine Database (http://goldmine.mib.infn.it/), and the Reference Catalog of galaxy Spectral Energy Distributions (RCSED: http://rcsed.sai.msu.ru/catalog).

[24] http://sci.esa.int/lisa-pathfinder/

Table 3. *CXO* observations of galaxies with a central X-ray point-source, and which are additionally expected to house a central black hole with mass $\lesssim 10^5\,M_\odot$.

Galaxy	Obs. Date	Exp. ksec	$F_{0.5-7\,\mathrm{keV}}$ (mod-indpt) 10^{-14} erg cm^{-2} s^{-1}	$F_{0.5-7\,\mathrm{keV}}$ (mod-dept) 10^{-14} erg cm^{-2} s^{-1}	$N_{H,Galaxy}$ 10^{20} cm^{-2}	$L_{0.5-8\,\mathrm{keV}}$ 10^{38} erg s^{-1}	$N_{H,intrin}$ 10^{22} cm^{-2}	Γ	kT_{in} keV	$L_{0.5-10\,\mathrm{keV}}$ 10^{38} erg s^{-1}	$L_{2-10\,\mathrm{keV}}$ 10^{38} erg s^{-1}
(1)	(2)	(3)	(4)	(5)	(6)	(7)	(8)	(9)	(10)	(11)	(12)
Presented in Graham et al. (2019)											
NGC 4178[a]	2011-02-19	36.29	0.50 (0.38–0.66)	0.56 (0.40–0.81)	2.66	4.04 (1.74–20.9)	$0.47^{+0.50}_{-0.35}$	$3.43^{+1.66}_{-1.24}$	...	4.06 (1.75–21.0)	0.51 (0.22–2.63)
NGC 4178[a]	2011-02-19	36.29	0.50 (0.38–0.66)	0.53 (0.38–0.73)	2.66	1.52 (0.96–2.77)	$0.15^{+0.33}_{-0.15}$	...	$0.56^{+0.35}_{-0.19}$	1.52 (0.96–2.77)	0.35 (0.22–0.65)
NGC 4713	2003-01-28	4.90	1.17 (0.65–1.91)	1.52 (0.86–2.43)	1.87	4.40 (2.48–7.02)	...	1.7	...	4.94 (2.79–7.88)	3.19 (1.80–5.09)
NGC 4470[b]	2010-11-20	19.78	0.42 (0.087–0.89)	0.35 (0.15–0.63)	1.60	1.31 (0.57–2.40)	...	1.7	...	1.47 (0.64–2.70)	0.95 (0.41–1.74)
New X-ray data											
NGC 4197	2018-07-27	7.96	11.20 (8.84–13.60)	10.60 (9.20–13.80)	1.52	119 (88.0–174)	$0.35^{+0.72}_{-0.35}$	$1.24^{+0.84}_{-0.69}$	...	144 (106–210)	113 (84–166)
NGC 4212[b]	2017-02-14	14.86	0.43 (0.19–0.79)	0.49 (0.22–0.90)	2.67	1.90 (0.87–3.48)	...	1.7	...	2.13 (0.98–3.91)	1.38 (0.63–2.52)
NGC 4298	2018-04-09	7.81	2.68 (1.55–4.22)	1.84 (1.08–2.88)	2.62	6.10 (3.59–9.56)	...	1.7	...	6.85 (4.03–10.74)	4.42 (2.60–6.93)
NGC 4313[b]	2018-04-14	7.96	0.55 (0.23–1.06)	0.87 (0.39–1.64)	2.40	2.32 (1.03–4.35)	...	1.7	...	2.61 (1.16–4.89)	1.68 (0.75–3.15)
NGC 4330	2018-04-16	7.96	6.30 (4.40–8.65)	6.55 (4.47–9.25)	2.07	80.7 (49.0–129.3)	$4.33^{+2.86}_{-1.96}$	1.7	...	90.6 (55.0–145.2)	58.5 (35.5–93.7)
NGC 4492[b]	2007-02-22	4.89	0.69 (0.29–1.32)	1.31 (0.65–2.32)	1.43	6.77 (3.19–13.35)	$0.05^{+0.25}_{-0.05}$	1.7	...	7.60 (3.58–14.99)	4.91 (2.31–9.68)
NGC 4492[b]	2014-04-25	29.68	0.54 (0.32–0.84)	0.85 (0.51–1.31)	1.43	4.40 (2.51–7.21)	$0.05^{+0.25}_{-0.05}$	1.7	...	4.94 (2.82–8.10)	3.19 (1.82–5.23)
NGC 4498	2018-04-07	8.09	0.60 (0.30–1.04)	1.17 (0.60–2.02)	2.25	3.29 (1.67–5.66)	...	1.7	...	3.69 (1.88–6.36)	2.39 (1.21–4.10)
NGC 4519	2018-05-05	8.45	1.10 (0.61–1.79)	1.39 (0.78–2.28)	1.36	7.02 (3.90–11.46)	...	1.7	...	7.88 (4.38–12.87)	5.09 (2.83–8.31)
NGC 4607	2018-05-09	7.96	4.93 (3.01–7.15)	3.84 (2.25–6.04)	2.53	51.0 (24.7–100.3)	$4.68^{+5.86}_{-2.64}$	1.7	...	57.3 (27.7–112.6)	37.9 (17.9–72.7)
Containing central X-ray emission, probably a point-source											
NGC 4405[c]	2018-04-09	7.96	0.62 (0.26–1.19)	0.84 (0.36–1.60)	2.17	3.54 (1.51–6.76)	...	1.7	...	3.98 (1.70–7.59)	2.57 (1.09–4.90)
NGC 4413[c]	2018-05-10	7.80	0.36 (0.14–0.69)	1.00 (0.46–1.84)	2.32	3.41 (1.57–6.26)	...	1.7	...	3.83 (1.76–7.59)	2.47 (1.14–4.54)

Column 1: [a] GSD19 reported that a blackbody curve fit the SED better than a power-law model. [b] For galaxies with a dual X-ray point-source, we are reporting the flux from the more central source. [c] Low photon count but probably a point-source. Column 4: The observed, i.e. partially-absorbed, model-independent, photon flux is for the centrally-located X-ray point-source in the *CXO*/ACIS-S 0.5–7 keV bands. The associated uncertainties show the 90% confidence range. Column 5: Absorbed model flux. Column 6: Galactic column density of neutral atomic hydrogen, H_I, (HI4PI Collaboration et al. 2016). Column 7: The X-ray luminosity $L_{0.5-8\,\mathrm{keV}}$ represents the unabsorbed 0.5–8 keV luminosity of each point-source, derived using the distances provided in Table 1 and corrected for our Galaxy's obscuring H_I plus (when indicated in column 8) the obscuring line-of-sight H_I intrinsic to the external galaxy. Column 9: The measured or adopted X-ray SED power-law slope, Γ. With $\Gamma = 1.7$, one has that $L_{0.5-8\,\mathrm{keV}} = 1.075\,L_{0.5-7\,\mathrm{keV}}$, and $L_{0.5-10\,\mathrm{keV}} = 1.20\,L_{0.5-7\,\mathrm{keV}}$, Column 10 gives the blackbody temperature of the model's inner disk (*diskbb*). Column 11: Unabsorbed X-ray luminosity $L_{0.3-10\,\mathrm{keV}}$ from 0.3–10 keV based on the extrapolated power-law SED.

REFERENCES

Abbott B. P., et al., 2016a, Living Reviews in Relativity, 19, 1
Abbott B. P., et al., 2016b, ApJ, 826, L13
Abbott B. P., et al., 2018, Living Reviews in Relativity, 21, 3
Abramovici A., et al., 1992, Science, 256, 325
Abramson A., Kenney J. D. P., Crowl H. H., Chung A., van Gorkom J. H., Vollmer B., Schiminovich D., 2011, AJ, 141, 164
Acernese F., et al., 2015, Classical and Quantum Gravity, 32, 024001
Alam S., et al., 2015, ApJS, 219, 12
Andreoni I., et al., 2017, Publ. Astron. Soc. Australia, 34, e069
Anza S., et al., 2005, Classical and Quantum Gravity, 22, S125
Armas Padilla M., Degenaar N., Russell D. M., Wijnand s R., 2013, MNRAS, 428, 3083
Arnaud K. A., 1996, in Jacoby G. H., Barnes J., eds, Astronomical Society of the Pacific Conference Series Vol. 101, Astronomical Data Analysis Software and Systems V. p. 17
Arnaud K., Smith R., Siemiginowska A., 2011, Handbook of X-ray Astronomy. Cambridge Observing Handbooks for Research Astronomers, Cambridge University Press, doi:10.1017/CBO9781139034234
Aso Y., Michimura Y., Somiya K., Ando M., Miyakawa O., Sekiguchi T., Tatsumi D., Yamamoto H., 2013, Phys. Rev. D, 88, 043007
Babak S., et al., 2017, Phys. Rev. D, 95, 103012
Bahcall J. N., Kozlovsky B.-Z., Salpeter E. E., 1972, ApJ, 171, 467
Balcells M., Graham A. W., Domínguez-Palmero L., Peletier R. F., 2003, ApJ, 582, L79
Baldassare V. F., Reines A. E., Gallo E., Greene J. E., 2015, ApJ, 809, L14
Baldassare V. F., Reines A. E., Gallo E., Greene J. E., 2017, ApJ, 850, 196
Baldwin J. A., Phillips M. M., Terlevich R., 1981, PASP, 93, 5
Barausse E., Lapi A., 2020, Massive Black Hole Mergers (arXiv:2011.01994)
Barth A. J., Ho L. C., Rutledge R. E., Sargent W. L. W., 2004, ApJ, 607, 90
Barth A. J., Strigari L. E., Bentz M. C., Greene J. E., Ho L. C., 2009, ApJ, 690, 1031
Baumgardt H., Makino J., Ebisuzaki T., 2004, ApJ, 613, 1133
Bekki K., Chiba M., 2008, ApJ, 679, L89
Binggeli B., Sandage A., Tammann G. A., 1985, AJ, 90, 1681
Birchall K. L., Watson M. G., Aird J., 2020, MNRAS, 492, 2268
Blackburn J. K., 1995, in Shaw R. A., Payne H. E., Hayes J. J. E., eds, Astronomical Society of the Pacific Conference Series Vol. 77, Astronomical Data Analysis Software and Systems IV. p. 367
Böker T., Laine S., van der Marel R. P., Sarzi M., Rix H.-W., Ho L. C., Shields J. C., 2002, AJ, 123, 1389
Bond J. R., Arnett W. D., Carr B. J., 1984, ApJ, 280, 825
Bonetti M., Sesana A., 2020, arXiv e-prints, p. arXiv:2007.14403
Booth R. S., de Blok W. J. G., Jonas J. L., Fanaroff B., 2009, arXiv e-prints, p. arXiv:0910.2935
Brocksopp C., Fender R. P., Larionov V., Lyuty V. M., Tarasov A. E., Pooley G. G., Paciesas W. S., Roche P., 1999, MNRAS, 309, 1063
Brum C., et al., 2019, MNRAS, 486, 691
Burke-Spolaor S., et al., 2018, in Murphy E., ed., Astronomical Society of the Pacific Conference Series Vol. 517, Science with a Next Generation Very Large Array. p. 677
Cann J. M., Satyapal S., Abel N. P., Blecha L., Mushotzky R. F., Reynolds C. S., Secrest N. J., 2019, ApJ, 870, L2
Capetti A., Kharb P., Axon D. J., Merritt D., Baldi R. D., 2009, AJ, 138, 1990
Carilli C. L., et al., 2015, arXiv e-prints, p. arXiv:1510.06438
Carollo C. M., Stiavelli M., de Zeeuw P. T., Mack J., 1997, AJ, 114, 2366
Caron B., et al., 1997, Classical and Quantum Gravity, 14, 1461
Carr B. J., Bond J. R., Arnett W. D., 1984, ApJ, 277, 445
Casares J., Charles P. A., Naylor T., 1992, Nature, 355, 614
Casares J., Negueruela I., Ribó M., Ribas I., Paredes J. M., Herrero A., Simón-Díaz S., 2014, Nature, 505, 378
Cash W., 1979, ApJ, 228, 939
Chilingarian I. V., Zolotukhin I. Y., Katkov I. Y., Melchior A.-L., Rubtsov E. V., Grishin K. A., 2017, ApJS, 228, 14
Chilingarian I. V., Katkov I. Y., Zolotukhin I. Y., Grishin K. A., Beletsky Y., Boutsia K., Osip D. J., 2018, ApJ, 863, 1
Chung A., van Gorkom J. H., Kenney J. D. P., Vollmer B., 2007, ApJ, 659, L115
Ciambur B. C., 2016, Publ. Astron. Soc. Australia, 33, e062
Cloet-Osselaer A., De Rijcke S., Vandenbroucke B., Schroyen J., Koleva M., Verbeke R., 2014, MNRAS, 442, 2909
Collaboration G., et al., 2020, Detection of faint stars near SgrA* with GRAVITY (arXiv:2011.03058)
Conselice C. J., Bhatawdekar R., Palmese A., Hartley W. G., 2020, ApJ, 890, 8
Corbel S., Nowak M. A., Fender R. P., Tzioumis A. K., Markoff S., 2003, A&A, 400, 1007
Côté P., et al., 2004, ApJS, 153, 223
Côté P., et al., 2006, ApJS, 165, 57
Coughlin M. W., et al., 2019, ApJ, 885, L19
Dahari O., 1985, ApJS, 57, 643
Davis B. L., Graham A. W., 2020, MNRAS, submitted
Davis B. L., Graham A. W., Seigar M. S., 2017, MNRAS, 471, 2187
Davis B. L., Graham A. W., Cameron E., 2018, ApJ, 869, 113
Davis B. L., Graham A. W., Cameron E., 2019, ApJ, 873, 85
Davis T. A., et al., 2020, MNRAS, 496, 4061
Decarli R., Gavazzi G., Arosio I., Cortese L., Boselli A., Bonfanti C., Colpi M., 2007, MNRAS, 381, 136
Dewdney P. E., Hall P. J., Schilizzi R. T., Lazio T. J. L. W., 2009, IEEE Proceedings, 97, 1482
Doi A., Asada K., Fujisawa K., Nagai H., Hagiwara Y., Wajima K., Inoue M., 2013, ApJ, 765, 69
Dokuchaev V. I., Ozernoi L. M., 1981, Soviet Astronomy Letters, 7, 158
Dong A.-J., Wu Q., 2015, MNRAS, 453, 3447
Fabbiano G., Paggi A., Karovska M., Elvis M., Nardini E., Wang J., 2020, arXiv e-prints, p. arXiv:2009.01824
Falcke H., Körding E., Markoff S., 2004, A&A, 414, 895
Farinelli R., Ferrigno C., Bozzo E., Becker P. A., 2016, A&A, 591, A29
Ferrarese L., Merritt D., 2000, ApJ, 539, L9
Ferrarese L., et al., 2006, ApJS, 164, 334
Ferrarese L., et al., 2012, ApJS, 200, 4
Ferrigno C., Becker P. A., Segreto A., Mineo T., Santangelo A., 2009, A&A, 498, 825
Filho M. E., Barthel P. D., Ho L. C., 2002, ApJS, 142, 223
Filippenko A. V., Sargent W. L. W., 1985, ApJS, 57, 503
Fischer T. C., et al., 2020, Fundamental Reference AGN Monitoring Experiment (FRAMEx) I: Jumping Out of the Plane with the VLBA (arXiv:2011.06570)
Foschini L., Rodriguez J., Fuchs Y., Ho L. C., Dadina M., Di Cocco G., Courvoisier T. J. L., Malaguti G., 2004, A&A, 416, 529
Fossati M., et al., 2018, A&A, 614, A57
Frank J., Rees M. J., 1976, MNRAS, 176, 633
Fruscione A., et al., 2006, in Society of Photo-Optical Instrumentation Engineers (SPIE) Conference Series. p. 62701V, doi:10.1117/12.671760
Gair J. R., Barack L., Creighton T., Cutler C., Larson S. L., Phinney E. S., Vallisneri M., 2004, Classical and Quantum Gravity, 21, S1595

Gair J. R., Mandel I., Miller M. C., Volonteri M., 2011, General Relativity and Gravitation, 43, 485
Galleti S., Federici L., Bellazzini M., Fusi Pecci F., Macrina S., 2004, A&A, 416, 917
Gallo E., Treu T., Jacob J., Woo J.-H., Marshall P. J., Antonucci R., 2008, ApJ, 680, 154
Gallo E., Treu T., Marshall P. J., Woo J.-H., Leipski C., Antonucci R., 2010, ApJ, 714, 25
Gaskin J. A., et al., 2019, Journal of Astronomical Telescopes, Instruments, and Systems, 5, 021001
Gebhardt K., et al., 2000, ApJ, 539, L13
Georgiev I. Y., Böker T., 2014, MNRAS, 441, 3570
Georgiev I. Y., Böker T., Leigh N., Lützgendorf N., Neumayer N., 2016, MNRAS, 457, 2122
González Delgado R. M., Pérez E., Tadhunter C., Vilchez J. M., José Miguel Rodríguez-Espinosa a., 1997, ApJS, 108, 155
González Delgado R. M., Pérez E., Cid Fernand es R., Schmitt H., 2008, AJ, 135, 747
Graham A. W., 2016, in Meiron Y., Li S., Liu F. K., Spurzem R., eds, IAU Symposium Vol. 312, Star Clusters and Black Holes in Galaxies across Cosmic Time. pp 269–273 (arXiv:1412.5715), doi:10.1017/S1743921315008017
Graham A. W., 2020, MNRAS, 492, 3263
Graham A. W., Driver S. P., 2007, ApJ, 655, 77
Graham A. W., Guzmán R., 2003, AJ, 125, 2936
Graham A. W., Scott N., 2015, ApJ, 798, 54
Graham A. W., Soria R., 2019, MNRAS, 484, 794
Graham A. W., Spitler L. R., 2009, MNRAS, 397, 2148
Graham A. W., Onken C. A., Athanassoula E., Combes F., 2011, MNRAS, 412, 2211
Graham A. W., Spitler L. R., Forbes D. A., Lisker T., Moore B., Janz J., 2012, ApJ, 750, 121
Graham A. W., Ciambur B. C., Soria R., 2016, ApJ, 818, 172
Graham A. W., Soria R., Davis B. L., 2019, MNRAS, 484, 814
Green J., Van Langevelde H. J., Brunthaler A., Ellingsen S., Imai H., Vlemmings W. H. T., Reid M. J., Richards A. M. S., 2015, in Advancing Astrophysics with the Square Kilometre Array (AASKA14). p. 119 (arXiv:1504.00485)
Greene J. E., Ho L. C., 2007, ApJ, 670, 92
Greenhill L. J., Kondratko P. T., Lovell J. E. J., Kuiper T. B. H., Moran J. M., Jauncey D. L., Baines G. P., 2003, ApJ, 582, L11
Gültekin K., Cackett E. M., Miller J. M., Di Matteo T., Markoff S., Richstone D. O., 2009, ApJ, 706, 404
Gültekin K., King A. L., Cackett E. M., Nyland K., Miller J. M., Di Matteo T., Markoff S., Rupen M. P., 2019, ApJ, 871, 80
Gursky H., Kellogg E. M., Leong C., Tananbaum H., Giacconi R., 1971, ApJ, 165, L43
HI4PI Collaboration et al., 2016, A&A, 594, A116
Hannikainen D. C., Hunstead R. W., Campbell-Wilson D., Sood R. K., 1998, A&A, 337, 460
Harry G. M., LIGO Scientific Collaboration 2010, Classical and Quantum Gravity, 27, 084006
Ho L. C., Filippenko A. V., Sargent W. L., 1995, ApJS, 98, 477
Ho L. C., Filippenko A. V., Sargent W. L. W., 1997, ApJS, 112, 315
Ho L. C., Greene J. E., Filippenko A. V., Sargent W. L. W., 2009, ApJS, 183, 1
Homan J., Belloni T., 2005, Ap&SS, 300, 107
Horner S. D., Rieke M. J., 2004, in Mather J. C., ed., Society of Photo-Optical Instrumentation Engineers (SPIE) Conference Series Vol. 5487, Optical, Infrared, and Millimeter Space Telescopes. pp 628–634, doi:10.1117/12.552281
Hough D. H., Vermeulen R. C., Readhead A. C. S., Cross L. L., Barth E. L., Yu L. H., Beyer P. J., Phifer E. M., 2002, AJ, 123, 1258
Huerta E. A., Gair J. R., 2011, Phys. Rev. D, 83, 044020
Humphreys E. M. L., Vlemmings W. H. T., Impellizzeri C. M. V., Galametz M., Olberg M., Conway J. E., Belitsky V., De Breuck C., 2016, A&A, 592, L13
Hutchings J. B., Crampton D., Campbell B., 1984, ApJ, 280, 41
Illarionov A. F., Romanova M. M., 1988, Azh, 65, 682
Jiang N., et al., 2018, ApJ, 869, 49
Jonas J. L., 2009, IEEE Proceedings, 97, 1522
Karachentsev I. D., Karachentseva V. E., Parnovskij S. L., 1993, Astronomische Nachrichten, 314, 97
Kawamura S., et al., 2011, Classical and Quantum Gravity, 28, 094011
Kewley L. J., Groves B., Kauffmann G., Heckman T., 2006, MNRAS, 372, 961
Komossa S., Burwitz V., Hasinger G., Predehl P., Kaastra J. S., Ikebe Y., 2003, ApJ, 582, L15
Koposov S. E., et al., 2020, MNRAS, 491, 2465
Kraft R. P., Burrows D. N., Nousek J. A., 1991, ApJ, 374, 344
Kuo C. Y., et al., 2011, ApJ, 727, 20
La Franca F., et al., 2015, MNRAS, 449, 1526
Lamperti I., et al., 2017, MNRAS, 467, 540
Larkin J. E., et al., 2016, in Ground-based and Airborne Instrumentation for Astronomy VI. p. 99081W (arXiv:1608.01720), doi:10.1117/12.2232212
Larsen S. S., Romanowsky A. J., Brodie J. P., Wasserman A., 2020, arXiv e-prints, p. arXiv:2010.07395
Levin Y., 2006, ApJ, 653, 1203
Li D., Nan R., Pan Z., 2013, in van Leeuwen J., ed., IAU Symposium Vol. 291, Neutron Stars and Pulsars: Challenges and Opportunities after 80 years. pp 325–330 (arXiv:1210.5785), doi:10.1017/S1743921312024015
Lin D., et al., 2020, ApJ, 892, L25
Liu X., Han Z., Zhang Z., 2016, Ap&SS, 361, 9
Liu H.-Y., Yuan W., Dong X.-B., Zhou H., Liu W.-J., 2018, ApJS, 235, 40
Lusso E., et al., 2012, MNRAS, 425, 623
Makarov D., Karachentsev I., 2011, MNRAS, 412, 2498
Manzano-King C. M., Canalizo G., Sales L. V., 2019, ApJ, 884, 54
Mapelli M., Ripamonti E., Vecchio A., Graham A. W., Gualandris A., 2012, A&A, 542, A102
Martínez-Palomera J., Lira P., Bhalla-Ladd I., Förster F., Plotkin R. M., 2020, ApJ, 889, 113
Matthews L. D., et al., 1999, AJ, 118, 208
McDermid R. M., et al., 2020, arXiv e-prints, p. arXiv:2009.09242
McGregor P. J., et al., 2012, in Ground-based and Airborne Instrumentation for Astronomy IV. p. 84461I, doi:10.1117/12.925259
McNamara P., et al., 2013, in Auger G., Binétruy P., Plagnol E., eds, Astronomical Society of the Pacific Conference Series Vol. 467, 9th LISA Symposium. p. 5
Merloni A., Heinz S., di Matteo T., 2003, MNRAS, 345, 1057
Merritt D., 2000, in Combes F., Mamon G. A., Charmandaris V., eds, Astronomical Society of the Pacific Conference Series Vol. 197, Dynamics of Galaxies: from the Early Universe to the Present. p. 221 (arXiv:astro-ph/9910546)
Merritt D., 2013, Dynamics and Evolution of Galactic Nuclei. Princeton: Princeton University Press
Merritt D., 2015, ApJ, 814, 57
Merritt D., Ferrarese L., 2001, in Knapen J. H., Beckman J. E., Shlosman I., Mahoney T. J., eds, Astronomical Society of the Pacific Conference Series Vol. 249, The Central Kiloparsec of Starbursts and AGN: The La Palma Connection. p. 335 (arXiv:astro-ph/0107134)
Mezcua M., Domínguez Sánchez H., 2020, ApJ, 898, L30
Mezcua M., Civano F., Marchesi S., Suh H., Fabbiano G., Volonteri M., 2018, MNRAS, 478, 2576
Miyoshi M., Moran J., Herrnstein J., Greenhill L., Nakai N., Diamond P., Inoue M., 1995, Nature, 373, 127
Moran E. C., Shahinyan K., Sugarman H. R., Vélez D. O., Era-

cleous M., 2014, AJ, 148, 136
Motta S., Belloni T., Homan J., 2009, MNRAS, 400, 1603
Mushotzky R., 2018, in den Herder J.-W. A., Nikzad S., Nakazawa K., eds, Society of Photo-Optical Instrumentation Engineers (SPIE) Conference Series Vol. 10699, Space Telescopes and Instrumentation 2018: Ultraviolet to Gamma Ray. p. 1069929 (arXiv:1807.02122), doi:10.1117/12.2310003
Nagar N. M., Falcke H., Wilson A. S., 2005, A&A, 435, 521
Nan R., 2006, Science in China: Physics, Mechanics and Astronomy, 49, 129
Nandra K., et al., 2013, arXiv e-prints, p. arXiv:1306.2307
Narayan R., Yi I., 1995, ApJ, 452, 710
Nguyen D. D., et al., 2017, ApJ, 836, 237
Nguyen D. D., et al., 2018, ApJ, 858, 118
Nguyen D. D., et al., 2019, ApJ, 872, 104
Nisbet D. M., Best P. N., 2016, MNRAS, 455, 2551
Nowak N., Saglia R. P., Thomas J., Bender R., Pannella M., Gebhardt K., Davies R. I., 2007, MNRAS, 379, 909
Oka T., Tsujimoto S., Iwata Y., Nomura M., Takekawa S., 2017, Nature Astronomy, 1, 709
Onken C. A., Ferrarese L., Merritt D., Peterson B. M., Pogge R. W., Vestergaard M., Wandel A., 2004, ApJ, 615, 645
Onken C. A., et al., 2014, ApJ, 791, 37
Paragi Z., et al., 2015, in Advancing Astrophysics with the Square Kilometre Array (AASKA14). p. 143 (arXiv:1412.5971)
Pastorini G., et al., 2007, A&A, 469, 405
Paturel G., Petit C., Prugniel P., Theureau G., Rousseau J., Brouty M., Dubois P., Cambrésy L., 2003, A&A, 412, 45
Paudel S., Smith R., Yoon S. J., Calderón-Castillo P., Duc P.-A., 2018, ApJS, 237, 36
Peebles P. J. E., 1972, ApJ, 178, 371
Penny S. J., et al., 2018, MNRAS, 476, 979
Peterson B. M., Wandel A., 2000, ApJ, 540, L13
Peterson B. M., et al., 2004, ApJ, 613, 682
Pfister H., Volonteri M., Dai J. L., Colpi M., 2020, MNRAS, 497, 2276
Pintore F., Zampieri L., Stella L., Wolter A., Mereghetti S., Israel G. L., 2017, ApJ, 836, 113
Plotkin R. M., Markoff S., Kelly B. C., Körding E., Anderson S. F., 2012, MNRAS, 419, 267
Plotkin R. M., Gallo E., Jonker P. G., 2013, ApJ, 773, 59
Plotkin R. M., et al., 2017, ApJ, 834, 104
Pounds K. A., Nandra K., Stewart G. C., George I. M., Fabian A. C., 1990, Nature, 344, 132
Pringle J. E., Rees M. J., 1972, A&A, 21, 1
Punturo M., et al., 2010, Classical and Quantum Gravity, 27, 194002
Quinlan G. D., Shapiro S. L., 1990, ApJ, 356, 483
Rau A., et al., 2013, arXiv e-prints, p. arXiv:1308.6785
Ravi V., Vedantham H., Phinney E. S., 2018, MNRAS, 478, L72
Reaves G., 1983, ApJS, 53, 375
Regan J. A., Wise J. H., Woods T. E., Downes T. P., O'Shea B. W., Norman M. L., 2020, arXiv e-prints, p. arXiv:2008.08090
Reitze D., et al., 2019, in Bulletin of the American Astronomical Society. p. 35 (arXiv:1907.04833)
Roediger J. C., Courteau S., 2015, MNRAS, 452, 3209
Russell T. D., White R. L., Long K. S., Blair W. P., Soria R., Winkler P. F., 2020, MNRAS, 495, 479
Sahu N., Graham A. W., Davis B. L., 2019a, ApJ, 876, 155
Sahu N., Graham A. W., Davis B. L., 2019b, ApJ, 887, 10
Sandage A., Binggeli B., Tammann G. A., 1985, AJ, 90, 1759
Sartori L. F., Schawinski K., Treister E., Trakhtenbrot B., Koss M., Shirazi M., Oh K., 2015, MNRAS, 454, 3722
Satyapal S., Böker T., Mcalpine W., Gliozzi M., Abel N. P., Heckman T., 2009, ApJ, 704, 439
Scarlata C., et al., 2004, AJ, 128, 1124
Secrest N. J., Satyapal S., Gliozzi M., Cheung C. C., Seth A. C., Böker T., 2012, ApJ, 753, 38
Seigar M. S., Kennefick D., Kennefick J., Lacy C. H. S., 2008, ApJ, 678, L93
Sérsic J. L., 1973, PASP, 85, 103
Sesana A., Haardt F., Madau P., 2006, ApJ, 651, 392
Seth A., Agüeros M., Lee D., Basu-Zych A., 2008, ApJ, 678, 116
She R., Ho L. C., Feng H., 2017, ApJ, 835, 223
Silk J., 2017, ApJ, 839, L13
Sobolewska M. A., Papadakis I. E., Done C., Malzac J., 2011, MNRAS, 417, 280
Soria R., Wu K., 2003, A&A, 410, 53
Strader J., Chomiuk L., Maccarone T. J., Miller-Jones J. C. A., Seth A. C., Heinke C. O., Sivakoff G. R., 2012, ApJ, 750, L27
Subramanian S., Ramya S., Das M., George K., Sivarani T., Prabhu T. P., 2016, MNRAS, 455, 3148
Terashima Y., Hirata Y., Awaki H., Oyabu S., Gandhi P., Toba Y., Matsuhara H., 2015, ApJ, 814, 11
Thatte N. A., et al., 2016, in Ground-based and Airborne Instrumentation for Astronomy VI. p. 99081X, doi:10.1117/12.2230629
The Event Horizon Telescope Collaboration et al., 2019, ApJ, 875, L4
The LIGO Scientific Collaboration et al., 2020, arXiv e-prints, p. arXiv:2009.01075
Thornton C. E., Barth A. J., Ho L. C., Rutledge R. E., Greene J. E., 2008, ApJ, 686, 892
Tingay S. J., et al., 2000, AJ, 119, 1695
Tremou E., et al., 2018, ApJ, 862, 16
Tzanavaris P., Georgantopoulos I., 2007, A&A, 468, 129
Valencia-S. M., Zuther J., Eckart A., García-Marín M., Iserlohe C., Wright G., 2012, A&A, 544, A129
Veilleux S., Osterbrock D. E., 1987, ApJS, 63, 295
Vollmer B., et al., 2012, A&A, 537, A143
Wan Z., et al., 2020, Nature, 583, 768
Wang S., Liu J., Qiu Y., Bai Y., Yang H., Guo J., Zhang P., 2016, ApJS, 224, 40
Wilkins S. M., Gonzalez-Perez V., Baugh C. M., Lacey C. G., Zuntz J., 2013, MNRAS, 431, 430
Willmer C. N. A., 2018, ApJS, 236, 47
Wood K. S., et al., 1984, ApJS, 56, 507
Woodgate B. E., et al., 1998, PASP, 110, 1183
Yang Q.-X., Xie F.-G., Yuan F., Zdziarski A. A., Gierliński M., Ho L. C., Yu Z., 2015, MNRAS, 447, 1692
Yee H. K. C., 1992, in Filippenko A. V., ed., Astronomical Society of the Pacific Conference Series Vol. 31, Relationships Between Active Galactic Nuclei and Starburst Galaxies. p. 417
Yozin C., Bekki K., 2012, ApJ, 756, L18
Yuan W., Zhou H., Dou L., Dong X. B., Fan X., Wang T. G., 2014, ApJ, 782, 55
Zackay B., Dai L., Venumadhav T., Roulet J., Zaldarriaga M., 2019, arXiv e-prints, p. arXiv:1910.09528
Zezas A., Birkinshaw M., Worrall D. M., Peters A., Fabbiano G., 2005, ApJ, 627, 711
Zhang H.-X., et al., 2020, ApJ, 891, L23
den Brok M., et al., 2015, ApJ, 809, 101
van Haarlem M. P., et al., 2013, A&A, 556, A2

This paper has been typeset from a TEX/LATEX file prepared by the author.